



# Rapid pathogen detection by metagenomic next-generation sequencing of infected body fluids

Wei Gu<sup>1,2,10</sup>, Xianding Deng<sup>1,2,10</sup>, Marco Lee<sup>3,10</sup>, Yasemin D. Sucu<sup>1,2</sup>, Shaun Arevalo<sup>1,2</sup>, Doug Stryke<sup>1,2</sup>, Scot Federman<sup>1,2</sup>, Allan Gopez<sup>1,2</sup>, Kevin Reyes<sup>1,2</sup>, Kelsey Zorn<sup>1,2</sup>, Hannah Sample<sup>4</sup>, Guixia Yu<sup>1,2</sup>, Gurpreet Ishpuniani<sup>1,2</sup>, Benjamin Briggs<sup>1,2</sup>, Eric D. Chow<sup>1,2</sup>, Amy Berger<sup>5</sup>, Michael R. Wilson<sup>1,2</sup>, Candace Wang<sup>1,2</sup>, Elaine Hsu<sup>1</sup>, Steve Miller<sup>1,2</sup>, Joseph L. DeRisi<sup>4,8</sup> and Charles Y. Chiu<sup>1,2,9</sup>

We developed a metagenomic next-generation sequencing (mNGS) test using cell-free DNA from body fluids to identify pathogens. The performance of mNGS testing of 182 body fluids from 160 patients with acute illness was evaluated using two sequencing platforms in comparison to microbiological testing using culture, 16S bacterial PCR and/or 28S-internal transcribed ribosomal gene spacer (28S-ITS) fungal PCR. Test sensitivity and specificity of detection were 79 and 91% for bacteria and 91 and 89% for fungi, respectively, by Illumina sequencing; and 75 and 81% for bacteria and 91 and 100% for fungi, respectively, by nanopore sequencing. In a case series of 12 patients with culture/PCR-negative body fluids but for whom an infectious diagnosis was ultimately established, seven (58%) were mNGS positive. Real-time computational analysis enabled pathogen identification by nanopore sequencing in a median 50-min sequencing and 6-h sample-to-answer time. Rapid mNGS testing is a promising tool for diagnosis of unknown infections from body fluids.

Early detection of causative microorganisms in patients with severe infection is critical to informing clinical interventions and the administration of appropriately targeted antibiotics<sup>1</sup>. Timely and accurate diagnosis, however, remains highly challenging for many hospitalized patients. Because most infectious syndromes present with indistinguishable clinical manifestations, broad-based, multiplexed diagnostic tests are urgently needed but are not yet available for the vast majority of potential pathogens. Some microorganisms are difficult to grow in culture (for example, *Treponema pallidum*, *Bartonella* spp.) or unculturable (for example, some viruses), while others (for example, mycobacteria and molds) can take weeks to grow and speciate<sup>2</sup>. Accurate molecular detection by PCR provides an alternative diagnostic approach to culture, but is hypothesis driven and thus requires a priori suspicion of the causative pathogen(s). Although PCR tests targeting the conserved 16S ribosomal RNA gene (16S PCR) and 28S-ITS PCR regions of bacteria and fungi, respectively, have been developed<sup>3,4</sup>, concerns have been raised regarding detection sensitivity<sup>5–7</sup>. Failure or delay in diagnosing infections results in extended hospitalizations and readmissions and increased mortality and morbidity<sup>8–10</sup>. In addition, patients who remain undiagnosed nearly always require empiric broad-spectrum therapy, with increased risk of adverse side effects and antimicrobial drug resistance<sup>11</sup>.

Metagenomic next-generation sequencing enables detection of nearly all known pathogens simultaneously from clinical samples<sup>12–14</sup>. Previous work in this area has focused on a single, generally

nonpurulent body fluid type<sup>7,14–24</sup> and few studies to date have demonstrated clinical validation and/or utility<sup>7,15,21,25,26</sup>. Methodology and sample types are also highly variable, making it difficult to evaluate comparative performance across different studies. In particular, purulent fluids, which often suggest an infectious etiology, can be challenging to analyze by mNGS due to high human host DNA background, which can decrease assay sensitivity<sup>20</sup>. Methods exist to enrich for pathogen-specific reads from metagenomic data, such as differential lysis of human cells<sup>16,17,23</sup>, but the scope of detection using these approaches is largely restricted to bacteria and/or fungi.

Rapid identification of pathogens from infected body fluid compartments is essential because empiric antimicrobial treatment is often suboptimal, contributing to increased morbidity and mortality<sup>8,25,27–29</sup>. Most metagenomic studies have employed Illumina sequencing platforms, with sequencing run times exceeding 16 h and overall sample-to-answer turnaround times of 48–72 h. In contrast, nanopore sequencing (MinION sequencer by Oxford Nanopore Technologies) can detect microbes within minutes of starting sequencing and with a turnaround time of <6 h (refs. 16,22,30). Nanopore sequencing has been used extensively for genomic surveillance of emerging viruses<sup>31–33</sup>, but clinical metagenomic applications of the technology for pathogen detection have been limited<sup>12</sup>. One published study describes the use of a saponin-based differential lysis enrichment method for metagenomic nanopore sequencing-based detection of bacteria in respiratory infections, with 96.6% sensitivity yet only 41.7% specificity<sup>16</sup>.

<sup>1</sup>Department of Laboratory Medicine, University of California San Francisco, San Francisco, CA, USA. <sup>2</sup>UCSF-Abbott Viral Diagnostics and Discovery Center, San Francisco, CA, USA. <sup>3</sup>Leeds Teaching Hospitals NHS Trust, Leeds, UK. <sup>4</sup>Department of Biochemistry and Biophysics, University of California San Francisco, San Francisco, CA, USA. <sup>5</sup>Department of Medicine, University of California San Francisco, San Francisco, CA, USA. <sup>6</sup>Weill Institute for Neurosciences, University of California San Francisco, San Francisco, CA, USA. <sup>7</sup>Department of Neurology, University of California San Francisco, San Francisco, CA, USA. <sup>8</sup>Chan Zuckerberg Biohub, San Francisco, CA, USA. <sup>9</sup>Department of Medicine, Division of Infectious Diseases, University of California San Francisco, San Francisco, CA, USA. <sup>10</sup>These authors contributed equally: Wei Gu, Xianding Deng, Marco Lee. e-mail: [charles.chiu@ucsf.edu](mailto:charles.chiu@ucsf.edu)

Here we describe a simple, rapid and universal method for pathogen detection by mNGS analysis of cell-free DNA (cfDNA) from a variety of different body fluids, ranging from low-cellularity cerebrospinal fluid (CSF) to purulent fluids with high human host DNA content (for example, abscesses). A new dual-use protocol, suitable for either Oxford Nanopore Technologies nanopore or Illumina sequencing platforms, is used to evaluate the diagnostic accuracy of mNGS testing against traditional culture and PCR-based testing. We also present a case series evaluating the performance of mNGS testing in 12 patients with culture- and PCR-negative body fluids. For all cases, there was either high clinical suspicion for an infectious etiology or a confirmed microbiological diagnosis by orthogonal laboratory testing.

## Results

**Sample collection.** A total of 182 body fluid samples from 160 patients, including 25 abscess, 21 joint, 32 pleural, 27 peritoneal, 35 cerebrospinal, 13 bronchoalveolar lavage (BAL) and 29 other body fluids (Table 1 and Supplementary Table 1), were collected as residual samples after routine clinical testing in the microbiology laboratory. Among these 182 samples, 170 were used to evaluate the accuracy of mNGS testing by Illumina sequencing (Fig. 1a and Supplementary Table 1). These accuracy samples included 127 positive by culture (with pathogen(s) identified to genus or species level), nine culture negative but positive by 16S or 28S-ITS PCR and 34 negative controls from patients with alternative noninfectious diagnoses (for example, cancer, trauma) (Fig. 1b). Out of the 170 samples used for evaluation of accuracy, the first 87 consecutively collected were used to compare the accuracy of nanopore relative to Illumina sequencing. The remaining 12 body fluid samples out of the 182 were collected from patients with negative direct microbiological testing of the body fluid but with highly suspected or orthogonally proven infection, as described in the case series section below (Fig. 1b, Table 2 and Supplementary Information). These 12 body fluid samples were analyzed to demonstrate the diagnostic utility of mNGS testing in the detection of pathogens in cases of unknown infectious etiology. Negative external controls (pooled donor plasma matrix) and positive external controls (donor plasma matrix spiked with known quantities of DNA from organisms considered nonpathogenic to humans) were run in parallel with body fluid samples (Supplementary Table 2).

**Study patients.** Among 158 patients out of 160 with available clinical data, 144 (91%) were hospitalized of whom 61 (39%) required intensive care unit management and 45 (28%) met clinical criteria for sepsis<sup>34</sup>; 51 (32%) were immunocompromised due to organ transplantation, recent chemotherapy, human immunodeficiency virus infection or drug-induced immunosuppression; and 71 (45%) were on antibiotics at the time of body fluid collection (Table 1). According to usual standard-of-care practices, bacterial cultures were obtained for all 182 body fluids with 63 (35%) and 81 (45%) having additional cultures done for acid-fast bacilli (AFB) and fungi, respectively.

**Metagenomic sequencing analysis.** We developed a dual-use bar-coding protocol for mNGS testing that was cross-compatible on both nanopore and Illumina sequencing platforms, suitable for all body fluids and automated in the clinical microbiology laboratory on liquid-handling workstations. The amount of input DNA varied over six logs, from approximately 100 pg ml<sup>-1</sup> in low-cellularity fluids such as CSF to 100 µg ml<sup>-1</sup> in purulent fluids. The median read depths for Illumina and nanopore sequencing were 7.2 M (interquartile range (IQR) 4.0–8.3 M, range 0.15–35 M) and 1.1 M (IQR 1.0–1.5 M, range 0.29–6.7 M), respectively (Supplementary Table 1). Metagenomic analysis for pathogen detection from Illumina data was performed using clinically validated sequence-based ultra-rapid

**Table 1 | Patient and sample characteristics**

Characteristics	Value
<b>Patient demographics (n = 158)</b>	
Age (years)	
Median (IQR)	54 (34–65)
Range	0–92
Gender, n (%)	
Female	75 (47)
Male	83 (53)
<b>Hospitalization, n (%)</b>	
Patients, total	158 (100)
In hospital	144 (91)
In intensive care unit	61 (39)
Days hospitalized, median (IQR)	14 (7–26)
30-day mortality, n (%)	9 (6)
Immunocompromised, n (%)	51 (32)
On empiric antibiotics at time of body fluid collection, n (%)	71 (45)
Sepsis according to SIRS criteria (>2), n (%) <sup>a</sup>	45 (28)
<b>Presumed illness, n (%)</b>	
Septic arthritis	21 (13)
Respiratory infection	39 (25)
Gastrointestinal abscess	15 (9)
Soft tissue abscess	18 (11)
Peritonitis	26 (16)
Central nervous system infection	32 (20)
Urinary tract infection	3 (2)
Eye infection	1 (0.6)
Other	3 (2)
<b>Sample characteristics (n = 182)</b>	
Sample type, n (%)	
Abscess	25 (14)
CSF	35 (19)
Joint fluid	21 (12)
Peritoneal fluid	27 (14)
Pleural fluid	32 (18)
BAL	13 (7)
Other <sup>b</sup>	29 (16)
WBC count of body fluid, median (IQR) ( $\times 10^6 \text{ l}^{-1}$ )	963 (161–1,925)
Range ( $\times 10^6 \text{ l}^{-1}$ )	1–382,000
Time to final culture result, median (IQR) (d)	4.8 (3.8–14.0)
Range (d)	1.3–35.7
Organism cultured, n (%)	
S. aureus	40 (22)
Streptococcus sp.	15 (8)
Enterococcus sp.	10 (5)
Gram-negative rods	30 (15)
Fungi	46 (23)
Other	20 (10)
Negative	35 (18)

<sup>a</sup>SIRS, systemic inflammatory response syndrome. <sup>b</sup>Vitreous fluid, perihepatic fluid, surgical swab, subgaleal fluid, heel fluid swab, perigraft fluid swab, anterior mediastinal fluid, chest fluid, chest wall mass, wound swab, synovial fluid, breast fluid, back fluid, fine needle aspirate, left thigh bursal fluid, perigastric fluid, thoracic spine seroma, peritonsillar drainage, knee swab, iliopsoas collection fluid, iliac wing fluid, retrogastric fluid and urine.

pathogen identification (SURPI+) software<sup>7,20</sup>. Nanopore sequencing yielded 1 million reads  $\text{h}^{-1}$  on average, with real-time data analysis performed using SURPI real-time (SURPIrt) software, a bioinformatics pipeline newly developed in-house for pathogen detection from metagenomic nanopore sequence data<sup>35</sup>. After a 5-h library preparation, nanopore sequencing detected pathogens in a median time of 50 min (IQR 23–80 min, range 21–320 min) (Fig. 1c and Supplementary Table 1), with an overall sample-to-answer turnaround time of ~6 h, whereas the turnaround time for Illumina sequencing was ~24 h. The time to pathogen detection on the nanopore platform was independent of body fluid type (Extended Data Fig. 1a), but was inversely correlated with estimated pathogen DNA titers based on reads per million (RPM) (Extended Data Fig. 1b).

**Test accuracy.** Accuracy evaluation focused on the performance of mNGS relative to gold standard culture and/or PCR testing for pathogen detection (Fig. 1a). For bacterial pathogen detection, two reference standards were applied in the evaluation: a clinical gold standard consisting of available culture and 16S PCR results and a composite standard that incorporated additional results from (1) orthogonal clinical testing of other sample types collected concurrently from the same patient, (2) confirmatory research-based digital PCR (dPCR) testing and (3) adjudication independently by an infectious disease specialist (C.Y.C.) and a clinical pathologist (W.G.). Adjudication was performed after mNGS results were available by integrating all sources of information, including longitudinal patient chart review and dPCR testing (Fig. 1a). Clinical samples were randomly divided into a training set ( $n=43$  samples, 36 bacterial organisms and eight fungal organisms) and a validation set ( $n=127$  samples, 85 bacteria and 32 fungi) for Illumina sequencing; and a training set ( $n=42$  samples, 34 bacteria and seven fungi) and validation set ( $n=43$  samples, 43 bacteria and 11 fungi) for nanopore sequencing. Receiver operator characteristic (ROC) and precision-recall curves for the training set were generated relative to the clinical and composite standards (Fig. 2a,b, Extended Data Fig. 1c–e and Supplementary Table 3). The curves were plotted using a normalized reads per million (nRPM) metric that adjusts RPM according to PCR cycle threshold (Methods).

At the optimal Youden's index (nRPM threshold of 2.6 and 0.54 for Illumina and nanopore sequencing, respectively) derived from the training set ROC curve, the sensitivity and specificity of mNGS testing for bacterial detection based on the validation set using the clinical gold standard were 79.2% (95% confidence interval (CI) 73.5–85.2%) and 90.6% (95% CI 87.3–93.8%), respectively, for Illumina sequencing, compared to 75.0% (95% CI 65.0–85.7%) and 81.4% (95% CI 74.1–89.3%), respectively, for nanopore sequencing (Fig. 2c). When using the composite standard, the positive percentage agreement (PPA) and negative percentage agreement (NPA) were 80.0% (95% CI 74.1–86.3%) and 95.3% (95% CI 92.9–97.6%), respectively, for Illumina sequencing compared to 81.0% (95% CI 72.4–89.7%) and 93.0% (95% CI 88.5–96.7%), respectively, for nanopore sequencing (Fig. 2c and Extended Data Fig. 2a,b). Excluding plasma, the performance of mNGS testing was comparable overall among different body fluid types (Fig. 2d), with the highest accuracy of detection from CSF. Nanopore sequencing yielded normalized read counts similar to Illumina sequencing ( $P=0.59$ ) (Fig. 2e). Stratification based on semiquantitation of culture colonies revealed significantly lower nRPM values for cultures grown from enrichment broth compared to other higher-titer cultures (rare, few, moderate, numerous colonies) ( $P=0.006$ ) (Extended Data Fig. 1f,g).

Among the 34 negative control samples that were negative by both culture and 16S PCR (Extended Data Fig. 1h), only one was a false positive for a bacterial pathogen above the nRPM detection threshold by mNGS (*Propionibacterium acnes*). Other reads from background contaminating organisms in negative control samples

were observed at levels below detection thresholds. Additional bacteria consisting of human commensal organisms, designated mNGS false positives relative to clinical gold standard testing, were also detected in 44% (7 of 16) and 20% (2 of 10) positive-control samples by Illumina and nanopore sequencing, respectively. The proportion of reads from each of these presumptive false-positive cases was <5% of the total number of microbial reads in the sample.

Among false-negative cases from both the training and validation set using the composite threshold, the most commonly missed organism was *Staphylococcus aureus* (Supplementary Table 1). Illumina sequencing missed 10 of 40 (25%) cases of *S. aureus*, but this was not statistically significant compared to missed cases of infection from other bacteria (12 of 81, 18%;  $P=0.21$ , Fisher's exact test) (Supplementary Table 4). Nanopore sequencing missed 10 of 26 (38.5%) cases of *S. aureus*, statistically significant compared to missed cases from other bacteria (4 of 50, 8%;  $P=0.0034$ , Fisher's exact test).

For fungal pathogen detection, a clinical gold standard consisting of available culture and 28S-ITS PCR results was used. On average, fungal DNA was at a significantly lower concentration based on nRPM counts than bacterial DNA ( $P=0.0049$ ) (Fig. 2f). At the optimal Youden's index derived from the training set ROC curve (nRPM = 0.1 for both Illumina and nanopore sequencing), the sensitivity and specificity of mNGS detection of fungi using an independent validation set were 90.6% (95% CI 84.2–100%) and 89.0% (95% CI 85.7–92.5%), respectively, for Illumina sequencing ( $n=127$  samples) compared to 90.9% (95% CI 80.0–100%) and 100%, respectively, for nanopore sequencing ( $n=43$  samples) (Fig. 2c, Extended Data Fig. 2c,d and Supplementary Table 5). Among the false-negative cases in the training and validation sets, at least one read corresponding to the fungal pathogen was detected in 57% (4 of 7) and 17% (1 of 6) samples by Illumina and nanopore sequencing, respectively, suggesting that sensitivity could potentially be boosted at greater depths of sequencing. The majority of fungal organisms (11 of 14, 79%) designated false positives by Illumina sequencing were found in <5% of all sequenced microbial reads in the sample.

**Limits of detection (LoD) and linearity.** We spiked DNA from a mixture of four organisms nonpathogenic to humans (*Streptococcus uberis*, *Rhodobacter sphaeroides*, *Millerozyma farinosa* and *Aspergillus oryzae*) into a healthy donor plasma matrix for LoD evaluation. Samples were spiked in fourfold dilutions, ranging from 1:1 (no dilution) to 1:4,096, with four replicates at each dilution. The LoD for bacterial detection using this assay was estimated to be 400–700 genome equivalents (GE)  $\text{ml}^{-1}$  for bacteria and 4 GE  $\text{ml}^{-1}$  for fungi (Supplementary Table 6). A strong linear correlation between organism titer (GE  $\text{ml}^{-1}$ ) and nRPM values by mNGS was observed ( $R^2=0.89\text{--}0.98$ ; Extended Data Fig. 3).

**Case series.** To assess the potential clinical utility of body fluid mNGS for diagnosis of infection, we selectively enrolled 12 patients with clinically probable or established infection despite negative culture and/or PCR testing of body fluid (Table 2). An infectious diagnosis had been made either by direct detection from a different body fluid/tissue or by serology/chemistry in eight and three cases, respectively. Peritoneal fluid from a patient with bowel perforation and suspected abdominal infection was also included. Presumptive causative pathogens (*Klebsiella aerogenes*, *Aspergillus fumigatus*, *Streptococcus pneumoniae*, *Streptococcus pyogenes*, *Cladophialophora psammophila*, *Candida parapsilosis* and anaerobic gastrointestinal microbiota) were identified in 7 of 12 cases using mNGS (Table 2 and Supplementary Information). Two additional cases of *T. pallidum* (neurosyphilis) and *Coccidioides immitis* (coccidioidomycosis), diagnosed by serology, had reads detected but present at levels below pre-established nRPM reporting thresholds<sup>4</sup>. Among the remaining three cases, mNGS testing was unable to

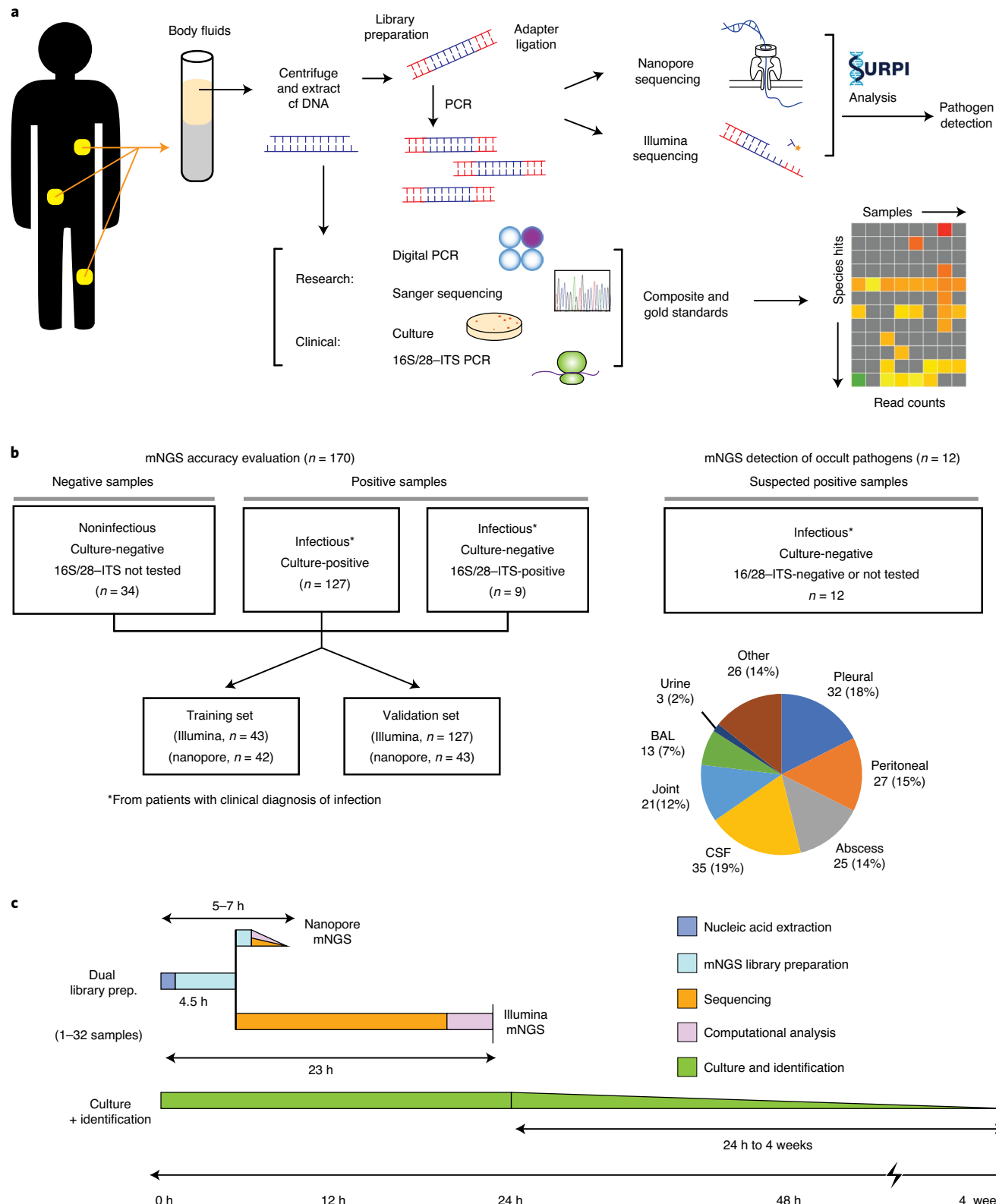


**Fig. 1 | Study workflow and sample distribution.** **a**, Schematic of mNGS body fluid analysis workflow. The clinical gold standard consisted of aggregated results from cultures, bacterial 16S PCR and/or fungal 28S-ITS PCR, while the composite standard also included confirmatory digital PCR with Sanger sequencing and clinical adjudication. For nanopore sequencing in <6 h, 40–60 min are needed for nucleic acid extraction, 2–2.5 h for mNGS library preparation, 1 h for nanopore 1D library preparation and 1 h for nanopore sequencing and analysis. **b**, Analysis workflow for the 182 body fluid samples included in the study; 170 samples were included in the accuracy assessment while 12 samples collected from patients with a clinical diagnosis of infection but negative microbiological testing were included for mNGS analysis. The pie chart displays the body fluid sample types analyzed in the study. \*From patients with clinical diagnosis of infection. **c**, Timing for mNGS testing relative to culture. Whereas culture-based pathogen identification can take days to weeks, mNGS testing using nanopore or Illumina sequencing platforms has an overall turnaround time of 5–24 h.

**Table 2 | Case series of body fluid mNGS testing in patients with probable or established infection but negative clinical microbiological testing**

Case no.	Body fluid sample type	Presentation	Body fluid mNGS result	Body fluid culture result	Body fluid 16S/28S-ITS PCR result <sup>a</sup>	Clinical microbiological diagnosis
S88	CSF	Encephalopathy without known cause; has a brain implant	Positive ( <i>K. aerogenes</i> )	Negative	Negative	<i>K. aerogenes</i> : same organism grown in culture from surgically removed DBS; concordant dPCR; matches clinical context
S89	Retroruterine fluid	Abdominal fluid collection and elevated WBC; a history of abdominal surgery	Positive (multiple gastrointestinal anaerobes) <sup>b</sup>	Negative	ND	None: mNGS results consistent with clinical context
S90	Pleural	Fever, cough, bacteremia, loculated pleural effusion	Positive ( <i>S. pneumoniae</i> )	Negative	ND	<i>S. pneumoniae</i> : concordant positive blood culture matches the clinical context
S91	Pleural	Fever, bacteremia, pneumonia, pleural effusion	Positive ( <i>S. pyogenes</i> )	Negative	ND	<i>S. pyogenes</i> : concordant positive blood culture matches the clinical context
S92	BAL	Pulmonary nodules post chemotherapy	Positive ( <i>A. fumigatus</i> )	Negative	ND	<i>A. fumigatus</i> : probable invasive aspergillosis matches clinical context; serum beta-D-glucan and serum galactomannan positive
S176	BAL	Cavitory lesion of the lung	Positive: below threshold ( <i>C. immitis</i> )	Negative	ND	<i>C. immitis</i> : serum coccidioides antibody positive, 1:16 titer on complement fixation
S177	CSF	Chronic meningoencephalitis	Positive ( <i>Cladophialophora bantiana</i> )	Negative	Negative	<i>C. bantiana</i> : brain tissue culture is positive for rare <i>C. bantiana</i>
S178	Pleural fluid	Cavitory lung lesions and pleural effusion	Negative <sup>c</sup>	Negative	ND	<i>C. neoformans</i> : BAL and bronchial wash fluid culture positive for <i>C. neoformans</i> ; serum cryptococcal antigen positive
S179	CSF	Headache, vision changes and optic disc edema	Positive: <i>T. pallidum</i> (below threshold)	ND	Negative	<i>T. pallidum</i> : serum rapid plasma reagin, venereal disease research laboratory and treponemal antibody positive
S180	Pleural fluid	Lymphadenopathy, lymphocytic pleural effusion	Negative <sup>c</sup>	Negative	ND	MTB: positive purified protein derivative; lymph node biopsy: necrotizing granulomas, AFB stain positive and MTB PCR positive
S181	CSF	Headaches, blurred vision, night sweats, neck stiffness	<i>Candida parasilopsis</i>	Negative	Negative	<i>C. parasilopsis</i> : serum beta-D-glucan >500 pg ml <sup>-1</sup> ; CSF culture 24 d later positive for <i>C. parasilopsis</i>
S182	CSF	Headache, photophobia, blurred vision, hydrocephalus	Negative <sup>c</sup>	Negative	Negative	<i>Sporothrix schenkii</i> : CSF (>1:16) and serum (1:32) <i>Sporothrix</i> antibody positive

<sup>a</sup>Bacterial 16S PCR or fungal 28S-ITS PCR. <sup>b</sup>The top five anaerobes were *Faecalibacterium prausnitzii*, *Eubacterium rectale*, *Akkermansia muciniphila*, *Acidaminococcus intestini* and *Bifidobacterium adolescentis*.<sup>c</sup>Infectious diagnosis missed by mNGS testing. ND, not done.

detect *Cryptococcus neoformans* in pleural fluid (diagnosis made from culture-positive BAL fluid), *Mycobacterium tuberculosis* (MTB) in pleural fluid (diagnosis made from a positive lymph node culture) and *Sporothrix* sp. in CSF (diagnosis made from serum and CSF IgM antibody positivity), presumably due to a lack of DNA representation from absent or very low pathogen titers and/or high human host background in the body fluid.

**Comparison of mNGS with bacterial 16S and fungal 28S-ITS PCR.** Out of the 160 patients, we compared the performance of mNGS relative to bacterial 16S PCR or fungal 28S-ITS PCR in 14 cases that had 16S or 28S-ITS PCR testing performed (Fig. 3 and Supplementary Table 7). At our hospital, bacterial 16S and fungal 28S-ITS PCR testing of body fluids and tissue is routinely ordered for culture-negative cases with high clinical suspicion for infection.

Concordant results between mNGS testing and PCR were obtained in 8 of 14 cases (Fig. 3a,b,d). Of the six discordant cases, five were found only by mNGS and one only by 16S PCR.

The first of three discordant bacterial cases was of an immunocompromised child with necrotizing pneumonia (case S31; Fig. 3c and Supplementary Information). 16S PCR testing of pleural fluid was positive for an organism in the *Streptococcus mitis* group, whereas mNGS testing identified *K. pneumoniae* (Fig. 3c). The finding of *K. pneumoniae* by mNGS was orthogonally validated as correct using five approaches: (1) dPCR of the DNA extract, (2) dPCR of the sequencing library, (3) Sanger sequencing of PCR amplicons from the DNA extract, (4) mNGS (Illumina) sequencing of the contralateral pleural fluid showing *K. pneumoniae* and (5) dPCR of the contralateral pleural fluid (Extended Data Fig. 4). In the second case, although culture and 16S PCR testing of the

body fluid (CSF) were both negative, a subsequent culture from a neurosurgically removed deep-brain stimulator (DBS) was positive for *K. aerogenes* (case S88; Fig. 3c and Supplementary Information). mNGS testing of CSF was also positive for *K. aerogenes*, a finding that was orthogonally validated by dPCR (Extended Data Fig. 5). We analyzed the length distribution of the pathogens detected by mNGS for these two cases using paired-end sequencing (Extended Data Fig. 6)<sup>36</sup>. The mean lengths of species-specific pathogen reads were 77 and 71 nucleotides (nt), with nearly all lengths <300 nt. The third discordant case was abscess fluid that was positive by 16S PCR for *Mycobacterium avium* complex but negative by mNGS testing.

In all three discordant fungal cases, body fluid mNGS was able to find the causative organism whereas fungal 28S–ITS PCR testing was negative (Fig. 3d). The causative organism had been clinically confirmed by culture of the same body fluid ( $n=1$ ), culture done 24 d later ( $n=1$ ) or testing of brain biopsy tissue ( $n=1$ ).

**Comparison of diagnostic yield of mNGS testing from body fluids versus plasma.** Seven patients in our study harboring a total of nine pathogens had paired body fluid and plasma samples available for comparative mNGS testing (Supplementary Table 8). Pathogen cfDNA burden based on nRPM was a median 160-fold higher (IQR 34–298) in local body fluid than in plasma from the same patient (Fig. 4 and Supplementary Table 8).

**Detection of anaerobic bacteria and viruses.** Anaerobic bacteria were not included in the accuracy assessment, because anaerobic culture was not always performed and cultured anaerobes were typically not speciated. However, the one sample in the accuracy study that was culture positive for an anaerobic bacterium (*Finegoldia magna* from a soft tissue abscess, case S87) was successfully detected by mNGS testing (Supplementary Table 9).

DNA viruses were also excluded from the accuracy assessment due to lack of routine clinical testing for viruses. Applying previously validated clinical mNGS thresholds of three nonoverlapping reads for viral detection<sup>20</sup>, 16 viruses were detected from the families Anelloviridae ( $n=5$ ), Herpesviridae ( $n=9$ ) and Adenoviridae ( $n=2$ ) (Supplementary Table 10). Four of the five (80%) anellovirus detections were from immunocompromised patients, consistent with the reported association of anelloviruses as nonpathogenic markers of active inflammation in this population<sup>37,38</sup>. Among the 11 remaining viruses detected by body fluid mNGS, six of six (100%) were orthogonally confirmed as true-positive cases by virus-specific PCR.

## Discussion

We describe a rapid diagnostic assay for unbiased metagenomic detection of DNA-based pathogens from body fluids. Key advances underlying our approach include (1) detection across a broad range of sample types, (2) compatibility with input cfDNA concentrations varying across six orders of magnitude (100 pg ml<sup>-1</sup>–100 ug ml<sup>-1</sup>),

(3) a dual-use barcoding system enabling deployment on Illumina and nanopore sequencing platforms and (4) clinically validated bioinformatics pipelines for automated analysis and interpretation of mNGS data. Importantly, we found that sensitivities and specificities for bacterial and fungal detection across Illumina and nanopore sequencing platforms are comparable. The potential utility of body fluid mNGS is highlighted by the detection of pathogens in 7 of 12 (58.3%) selected cases for which culture and PCR testing of the body fluid were negative, with subthreshold detection of pathogen reads in an additional two cases (9 of 12, 75%) (Table 2).

In this study, mNGS testing failed to detect *S. aureus* at higher rates than other bacteria, a finding that was statistically significant for nanopore but not for Illumina sequencing. We attribute the lower sensitivity of *S. aureus* detection by nanopore sequencing to higher levels of human host background DNA. Notably, the median body fluid white blood cell (WBC) count for *S. aureus* was  $70,250 \times 10^6 l^{-1}$  (IQR 42,800–137,500  $\times 10^6 l^{-1}$ ), an approximately 100-fold increase over median WBC counts for other microorganisms ( $P < 0.00001$  by Mann–Whitney *U*-test). Other factors contributing to lower sensitivity for nanopore sequencing may be the lower read depths achieved in the current study and higher error rates relative to Illumina sequencing. These limitations may potentially be addressed by increasing average sequencing throughput per sample or by ongoing improvements in nanopore read accuracy over time.

Our protocol relies on finding pathogen-specific cfDNA sequences in body fluid supernatant. Other groups have used host depletion methods, such as differential lysis, to enrich for intact pathogen DNA from high human DNA background samples, such as respiratory or joint fluids<sup>16,23</sup>. However, because the supernatant containing pathogen cfDNA is removed during the differential lysis protocol, such enrichment methods may not work well for low-cellularity samples such as plasma and CSF. Differential lysis can also hinder detection of other microorganisms such as viruses and parasites. In addition, these methods involve multiple steps of lysis and centrifugation, which can increase method complexity and prolong assay turnaround times. Our method also forgoes the use of mechanical processing steps such as bead beating. Bead beating may improve the detection of intact fungi and some bacteria containing rigid cell walls, but is laborious for routine use in the clinical laboratory and can reduce detection sensitivity by increasing host background from the release of human DNA.

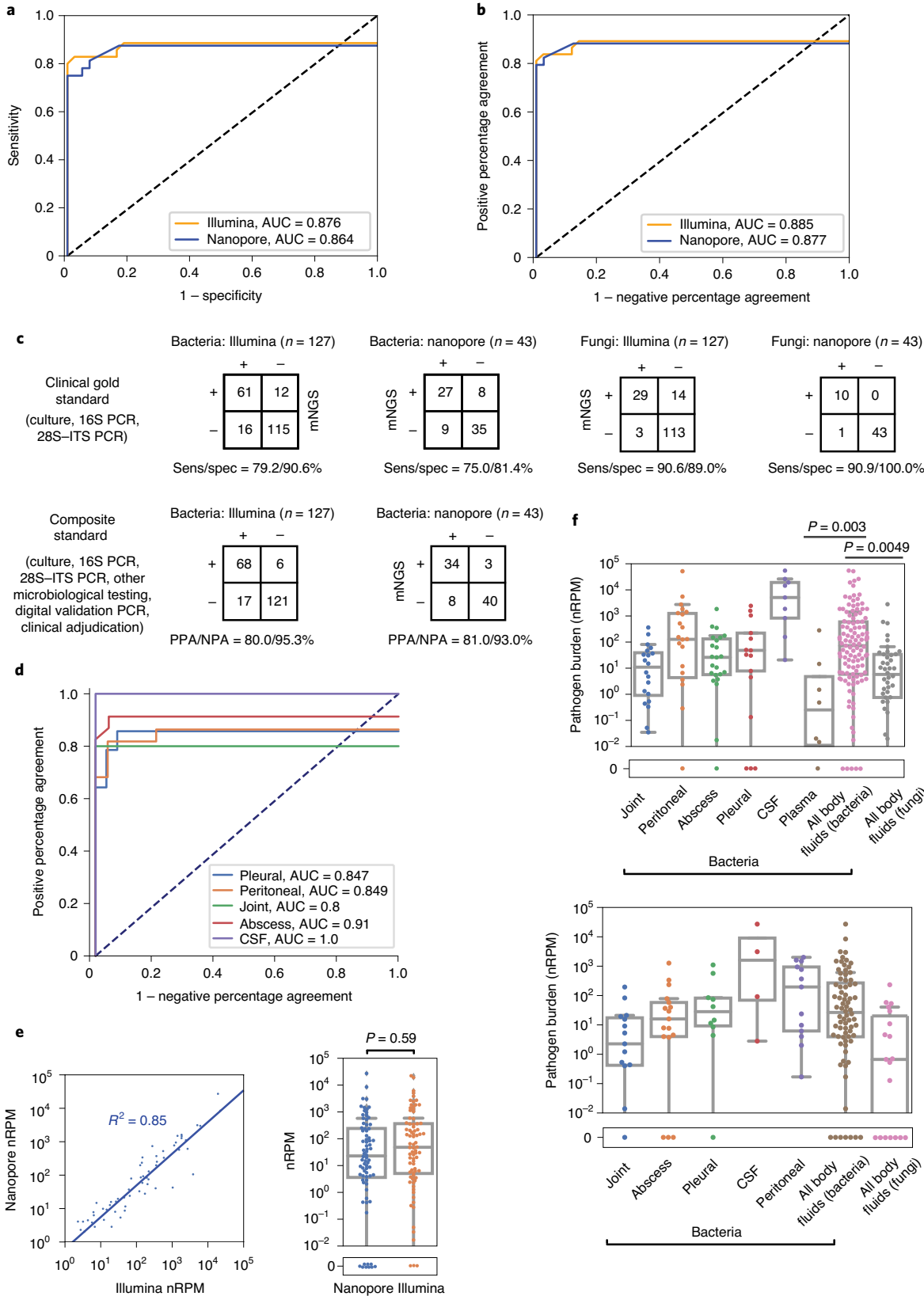
Previously published studies have used metagenomic sequencing for pathogen detection in sepsis and pneumonia<sup>15,16</sup>. However, the reported test specificities of 63 and 42.7%, respectively, may limit broad clinical application, as it can be challenging to evaluate the clinical significance of false-positive results. In contrast, an overall specificity ranging from 83 to 100% was achieved using our protocol.

Pathogen cfDNA analysis from blood has been used to diagnose deep-seated infections<sup>15,39–41</sup>. However, bacterial DNA is often present at low levels in blood, with a lower quartile of five bacterial

**Fig. 2 | Accuracy of mNGS testing and relative pathogen burden in body fluid samples.** **a**, ROC curves of Illumina ( $n=43$  samples) and nanopore ( $n=42$  samples) training sets based on culture and 16S testing. Plotted are mNGS test sensitivities and specificities, relative to the clinical gold standard, at nRPM threshold values ranging from 0.1 to 100. **b**, ROC curves of both training sets based on a composite standard. **c**, Contingency tables for the independent Illumina ( $n=127$  samples) and nanopore ( $n=43$  samples) validation sets. PPA and NPA are shown in lieu of sensitivity (sens) and specificity (spec), respectively, if a composite standard was used. The scoring system for determination of positive and negative results is described in Supplementary Table 12. **d**, ROC curves stratified by body fluid type ( $n=170$  samples in total). Plotted is the performance of the combined Illumina training and validation datasets relative to composite standard testing. **e**, Direct comparison of Illumina and nanopore sequencing ( $n=79$  bacteria) across all body fluids. The yield of pathogen-specific reads based on a nRPM metric is linearly correlated and comparable between nanopore and Illumina sequencing. **f**, Relative pathogen burden in body fluids, stratified by body fluid and microorganism type (upper, Illumina; lower, nanopore; total organisms,  $n=122$  and  $n=95$ , respectively). The burden of pathogen cfDNA in body fluid samples is estimated using calculated nRPM values. Based on Illumina data, bacterial cfDNA in plasma was significantly lower on average than in local body fluids ( $P=0.0035$ ), and pathogen cfDNA in body fluids was significantly higher for bacteria than for fungi ( $P=0.0049$ ). All box plots represent the median (center), the interquartiles (minima and maxima) and 1.5×IQR (whiskers). All *P* values are calculated using a two-sided Welch's *t*-test. **f**, Plasma is not counted as a body fluid but is plotted as a separate set. AUC, area under ROC curve.

genome copies per ml in patients with sepsis<sup>15</sup>. We show here that, in matched pairs of samples, there was an observed 160-fold higher pathogen cfDNA burden in body fluids. Similarly, tumor cfDNA is higher in adjacent body fluids than in blood<sup>42–46</sup>. Higher levels of

pathogen cfDNA in body fluids can increase analytical sensitivity and decrease the sequencing depths required for accurate detection, thereby lowering the cost of testing. In addition, direct identification of a pathogen from a body fluid can localize the source of an



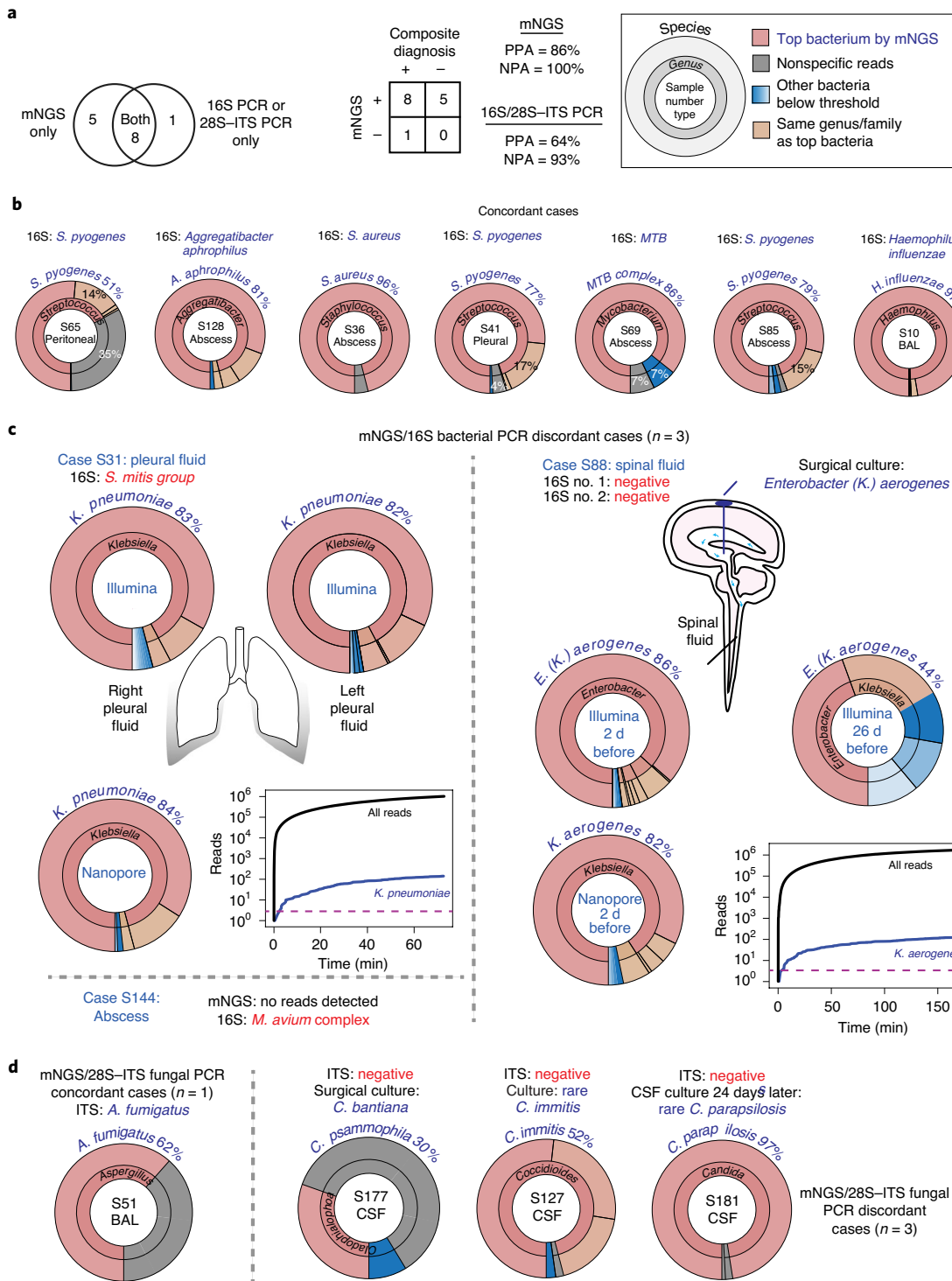


**Fig. 3 | Comparison of mNGS and 16S (bacterial) or 28S-ITS (fungal) PCR.** **a**, mNGS and 16S/28S-ITS PCR testing results for 14 culture-negative body fluid samples. The Venn diagram shows all cases out of 182 where mNGS and associated 16S or 28S-ITS PCR detected a microorganism. **b,c**, Krona plots depicting genus and species levels of all sequence-matched bacterial or fungal reads depending on the microorganism type: concordant bacterial cases ( $n = 7$  samples) (**b**) and discordant bacterial cases ( $n = 3$  samples) (**c**). In case S31 (top left), mNGS identified the causative pathogen in a case of necrotizing pneumonia (*K. pneumoniae*) whereas 16S PCR testing was falsely positive for *S. mitis*. In case S88 (right), mNGS identified *K. aerogenes* in CSF that tested negative by culture and 16S PCR, a finding confirmed by culture of an infected DBS located upstream of the lumbar puncture site (drawing and axial slice). Nanopore sequencing was able to detect both bacteria within 3 min of the start of sequencing (x-y plots with dashed line showing the detection threshold). In case S144 (bottom left), *M. avium* complex was detected by 16S PCR but not by mNGS. **d**, Fungal cases ( $n = 4$  samples, three discordant and one concordant). In the three discordant cases (right), mNGS testing detected the causative pathogen while 28S-ITS testing was negative. All three mNGS results were orthogonally confirmed by concurrent or subsequent culture of either body fluid or biopsy tissue. *C. bantiana* and *C. psammophila* are closely genetically related species. For additional details on these cases, see Supplementary Table 6 and Supplementary Information.

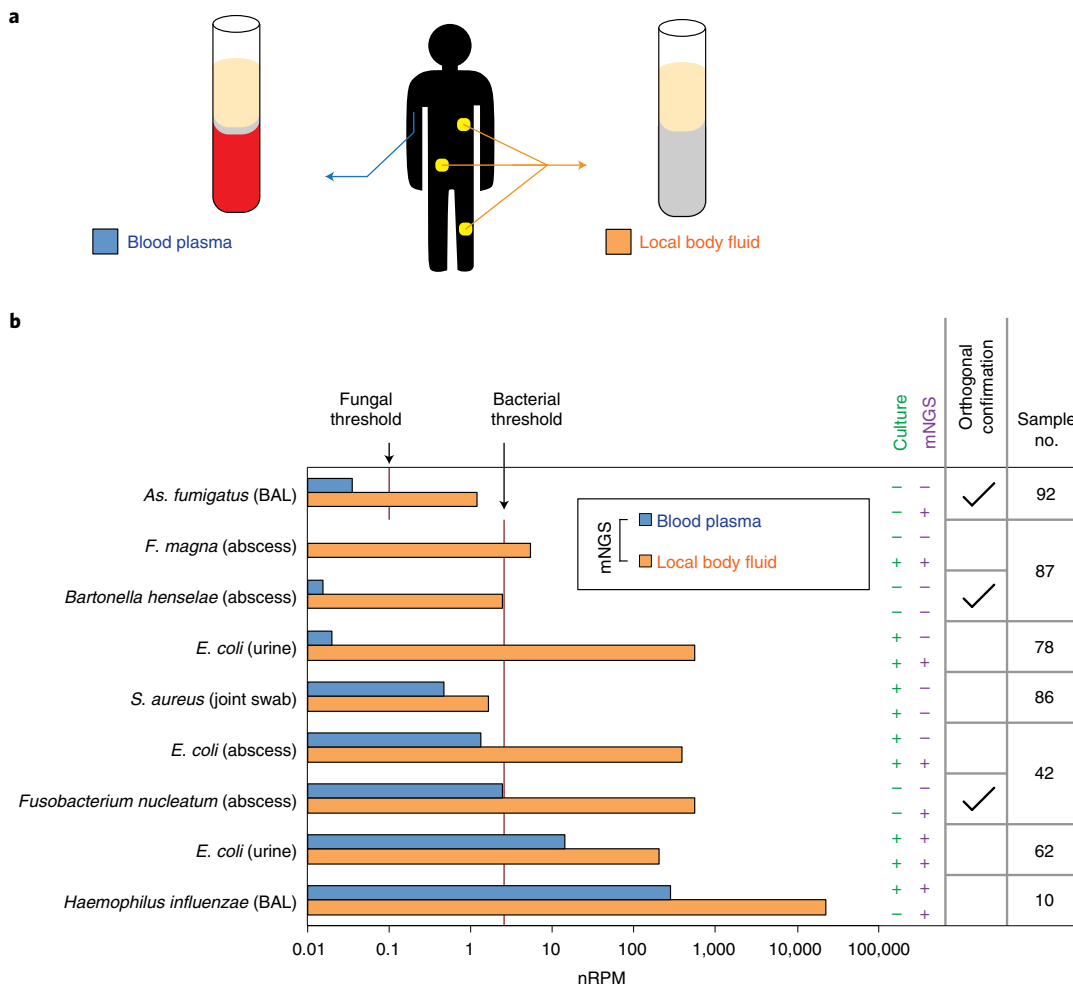


**Fig. 4 | Comparison of relative pathogen burden in paired body fluid and plasma samples.** **a**, Schematic showing concurrent collection of blood plasma and body fluid samples from the same patient. **b**, Bar plot of nRPM corresponding to nine organisms in paired body fluid and plasma samples from seven patients. The vertical lines denote the thresholds used for positive bacterial ( $nRPM = 2.6$ ) or fungal ( $nRPM = 0.1$ ) detection. The checkboxes denote microorganisms that were not identified by conventional microbiological testing (culture and/or 16S PCR) but that were orthogonally confirmed by dPCR, serology and/or clinical adjudication (Supplementary Information).

infection, which is critical to guiding definitive management and treatment.

In comparing mNGS with bacterial 16S or fungal 28S-ITS PCR, occult pathogens were detected solely by mNGS in 5 of 14 cases. False-negative 16S PCR results have previously been reported, and are generally attributed to suboptimal primer design<sup>6</sup> or decreased assay sensitivity from background contamination<sup>47</sup>. However, discordant results between 16S PCR and mNGS may also be due to short pathogen read lengths in cell-free body fluids (Extended Data Fig. 6). Notably, size ranges for bacterial 16S PCR amplicons span 300–460 nt (refs. <sup>48–50</sup>) whereas those for fungal 28S-ITS PCR amplicons span 250–650 nt (ref. <sup>51</sup>). Decreases in sensitivity due to fragmented cfDNA that are not amenable to long-read amplicon PCR have also been observed for detection of Epstein–Barr virus in clinical samples<sup>52</sup>.

Limitations of our study include the following. First, the numbers of each body fluid type tested were limited, ranging from 13 to 35 for the most common body fluid types. Second, clinical samples had varying depths of sequencing, which may have contributed to some of the false-negative results. Third, orthogonal testing such as bacterial 16S PCR or fungal 28S-ITS PCR was not performed on all samples. Fourth, neither external controls nor a large database of negative controls were used to normalize for microbial background, thus potentially reducing assay specificity. Fifth, convenience sam-

pling for collection of positive-control body fluids was performed based on availability (sufficient residual volume after clinical testing was completed).

In conclusion, here we demonstrate the utility of mNGS in expanding the scope of conventional diagnostic testing to multiple body fluid types. The achievable <6-h turnaround time using nanopore sequencing may also be essential for infections such as sepsis and pneumonia that demand a rapid response and timely diagnosis<sup>16,30</sup>. Traditionally, clinical mNGS has been performed late in the patient's disease course and as a test of last resort<sup>7,12</sup>. Nevertheless, our results suggest that clinical mNGS testing may be useful in at least four other scenarios: (1) for identification of culture-negative or slow-growing pathogens, (2) for diagnosis of rare or unusual infections that were not considered by the health care provider *a priori*<sup>6,53–56</sup>, (3) as a first-line test in critically ill patients and (4) as an early alternative to the large number of send-out tests that would otherwise be ordered as part of the diagnostic workup.

#### Online content

Any methods, additional references, Nature Research reporting summaries, source data, extended data, supplementary information, acknowledgements, peer review information; details of author contributions and competing interests; and statements of

data and code availability are available at <https://doi.org/10.1038/s41591-020-1105-z>.

Received: 16 January 2020; Accepted: 17 September 2020;  
Published online: 09 November 2020

## References

- Messacar, K., Parker, S. K., Todd, J. K. & Dominguez, S. R. Implementation of rapid molecular infectious disease diagnostics: the role of diagnostic and antimicrobial stewardship. *J. Clin. Microbiol.* **55**, 715–723 (2017).
- Rea, B., Maisel, J. R., Glaser, L. & Alby, K. Identification of clinically relevant mycobacterial species after extended incubation times in the BACTEC MGIT System. *Am. J. Clin. Pathol.* **151**, 63–67 (2019).
- Janda, J. M. & Abbott, S. L. 16S rRNA gene sequencing for bacterial identification in the diagnostic laboratory: pluses, perils, and pitfalls. *J. Clin. Microbiol.* **45**, 2761–2764 (2007).
- Petti, C. A., Polage, C. R. & Schreckenberger, P. The role of 16S rRNA gene sequencing in identification of microorganisms misidentified by conventional methods. *J. Clin. Microbiol.* **43**, 6123–6125 (2005).
- Reuwer, A. Q., van den Bijllaardt, W., Murk, J. L., Buiting, A. G. M. & Verweij, J. J. Added diagnostic value of broad-range 16S PCR on periprosthetic tissue and clinical specimens from other normally sterile body sites. *J. Appl. Microbiol.* **126**, 661–666 (2019).
- Wilson, M. R. et al. Actionable diagnosis of neuroleptospirosis by next-generation sequencing. *N. Engl. J. Med.* **370**, 2408–2417 (2014).
- Wilson, M. R. et al. Clinical metagenomic sequencing for diagnosis of meningitis and encephalitis. *N. Engl. J. Med.* **380**, 2327–2340 (2019).
- Glimaker, M. et al. Adult bacterial meningitis: earlier treatment and improved outcome following guideline revision promoting prompt lumbar puncture. *Clin. Infect. Dis.* **60**, 1162–1169 (2015).
- Kumar, A. et al. Duration of hypotension before initiation of effective antimicrobial therapy is the critical determinant of survival in human septic shock. *Crit. Care Med.* **34**, 1589–1596 (2006).
- Weiss, S. L. et al. Delayed antimicrobial therapy increases mortality and organ dysfunction duration in pediatric sepsis. *Crit. Care Med.* **42**, 2409–2417 (2014).
- Llor, C. & Bjerrum, L. Antimicrobial resistance: risk associated with antibiotic overuse and initiatives to reduce the problem. *Ther. Adv. Drug Saf.* **5**, 229–241 (2014).
- Chiu, C. Y. & Miller, S. A. Clinical metagenomics. *Nat. Rev. Genet.* **20**, 341–355 (2019).
- Gu, W., Miller, S. & Chiu, C. Y. Clinical metagenomic next-generation sequencing for pathogen detection. *Annu. Rev. Pathol.* **14**, 319–338 (2019).
- Simmer, P. J., Miller, S. & Carroll, K. C. Understanding the promises and hurdles of metagenomic next-generation sequencing as a diagnostic tool for infectious diseases. *Clin. Infect. Dis.* **66**, 778–788 (2018).
- Blauwkamp, T. A. et al. Analytical and clinical validation of a microbial cell-free DNA sequencing test for infectious disease. *Nat. Microbiol.* **4**, 663–674 (2019).
- Charalampous, T. et al. Nanopore metagenomics enables rapid clinical diagnosis of bacterial lower respiratory infection. *Nat. Biotechnol.* **37**, 783–792 (2019).
- Ivy, M. I. et al. Direct detection and identification of prosthetic joint infection pathogens in synovial fluid by metagenomic shotgun sequencing. *J. Clin. Microbiol.* **56**, e00402-18 (2018).
- Langelier, C. et al. Integrating host response and unbiased microbe detection for lower respiratory tract infection diagnosis in critically ill adults. *Proc. Natl Acad. Sci. USA* **115**, E12353–E12362 (2018).
- Leo, S. et al. Detection of bacterial pathogens from broncho-alveolar lavage by next-generation sequencing. *Int. J. Mol. Sci.* **18**, 2011 (2017).
- Miller, S. et al. Laboratory validation of a clinical metagenomic sequencing assay for pathogen detection in cerebrospinal fluid. *Genome Res.* **29**, 831–842 (2019).
- Schlaberg, R. et al. Validation of metagenomic next-generation sequencing tests for universal pathogen detection. *Arch. Pathol. Lab. Med.* **141**, 776–786 (2017).
- Schmidt, K. et al. Identification of bacterial pathogens and antimicrobial resistance directly from clinical urines using nanopore-based metagenomic sequencing. *J. Antimicrob. Chemother.* **72**, 104–114 (2017).
- Thoendel, M. J. et al. Identification of prosthetic joint infection pathogens using a shotgun metagenomics approach. *Clin. Infect. Dis.* **67**, 1333–1338 (2018).
- Wilson, M. R. et al. Chronic meningitis investigated via metagenomic next-generation sequencing. *JAMA Neurol.* **75**, 947–955 (2018).
- Lucas, M. J., Brouwer, M. C. & van de Beek, D. Neurological sequelae of bacterial meningitis. *J. Infect.* **73**, 18–27 (2016).
- Schlaberg, R. et al. Viral pathogen detection by metagenomics and pan-viral group polymerase chain reaction in children with pneumonia lacking identifiable etiology. *J. Infect. Dis.* **215**, 1407–1415 (2017).
- Costales, C. & Butler-Wu, S. M. A real pain: diagnostic quandaries and septic arthritis. *J. Clin. Microbiol.* **56**, e01358-17 (2018).
- McGill, F., Heyderman, R. S., Panagiotou, S., Tunkel, A. R. & Solomon, T. Acute bacterial meningitis in adults. *Lancet* **388**, 3036–3047 (2016).
- Singal, A. K., Salameh, H. & Kamath, P. S. Prevalence and in-hospital mortality trends of infections among patients with cirrhosis: a nationwide study of hospitalised patients in the United States. *Aliment. Pharm. Ther.* **40**, 105–112 (2014).
- Greninger, A. L. et al. Rapid metagenomic identification of viral pathogens in clinical samples by real-time nanopore sequencing analysis. *Genome Med.* **7**, 99 (2015).
- Faria, N. R. et al. Mobile real-time surveillance of Zika virus in Brazil. *Genome Med.* **8**, 97 (2016).
- Kafetzopoulou, L. E. et al. Metagenomic sequencing at the epicenter of the Nigeria 2018 Lassa fever outbreak. *Science* **363**, 74–77 (2019).
- Quick, J. et al. Real-time, portable genome sequencing for Ebola surveillance. *Nature* **530**, 228–232 (2016).
- Raith, E. P. et al. Prognostic accuracy of the SOFA Score, SIRS Criteria, and qSOFA score for in-hospital mortality among adults with suspected infection admitted to the intensive care unit. *JAMA* **317**, 290–300 (2017).
- Deng, X. et al. Metagenomic sequencing with spiked primer enrichment for viral diagnostics and surveillance. *Nat. Microbiol.* **5**, 443–454 (2020).
- Fan, H. C., Blumenfeld, Y. J., Chittikara, U., Hudgins, L. & Quake, S. R. Analysis of the size distributions of fetal and maternal cell-free DNA by paired-end sequencing. *Clin. Chem.* **56**, 1279–1286 (2010).
- De Vlaminck, I. et al. Temporal response of the human virome to immunosuppression and antiviral therapy. *Cell* **155**, 1178–1187 (2013).
- Focosi, D., Antonelli, G., Pistello, M. & Maggi, F. Torquenotavirus: the human virome from bench to bedside. *Clin. Microbiol. Infect.* **22**, 589–593 (2016).
- Abrial, M. K. et al. Diagnosis of *Capnocytophaga canimorsus* sepsis by whole-genome next-generation sequencing. *Open Forum Infect. Dis.* **3**, ofw144 (2016).
- Grumaz, S. et al. Next-generation sequencing diagnostics of bacteremia in septic patients. *Genome Med.* **8**, 73 (2016).
- Long, Y. et al. Diagnosis of sepsis with cell-free DNA by next-generation sequencing technology in ICU patients. *Arch. Med. Res.* **47**, 365–371 (2016).
- De Mattos-Arruda, L. et al. Cerebrospinal fluid-derived circulating tumour DNA better represents the genomic alterations of brain tumours than plasma. *Nat. Commun.* **6**, 8839 (2015).
- Dudley, J. C. et al. Detection and surveillance of bladder cancer using urine tumor DNA. *Cancer Discov.* **9**, 500–509 (2019).
- Pan, W., Gu, W., Nagpal, S., Gephart, M. H. & Quake, S. R. Brain tumor mutations detected in cerebral spinal fluid. *Clin. Chem.* **61**, 514–522 (2015).
- Springer, S. U. et al. Non-invasive detection of urothelial cancer through the analysis of driver gene mutations and aneuploidy. *eLife* **7**, e32143 (2018).
- Wang, Y. et al. Evaluation of liquid from the Papanicolaou test and other liquid biopsies for the detection of endometrial and ovarian cancers. *Sci. Transl. Med.* **10**, eaap8793 (2018).
- Corless, C. E. et al. Contamination and sensitivity issues with a real-time universal 16S rRNA PCR. *J. Clin. Microbiol.* **38**, 1747–1752 (2000).
- Klindworth, A. et al. Evaluation of general 16S ribosomal RNA gene PCR primers for classical and next-generation sequencing-based diversity studies. *Nucleic Acids Res.* **41**, e1 (2013).
- Salipante, S. J. et al. Performance comparison of Illumina and ion torrent next-generation sequencing platforms for 16S rRNA-based bacterial community profiling. *Appl. Environ. Microbiol.* **80**, 7583–7591 (2014).
- Wang, Y. & Qian, P. Y. Conservative fragments in bacterial 16S rRNA genes and primer design for 16S ribosomal DNA amplicons in metagenomic studies. *PLoS ONE* **4**, e7401 (2009).
- Hoggard, M. et al. Characterizing the human Mycobiota: a comparison of small subunit rRNA, ITS1, ITS2, and large subunit rRNA genomic targets. *Front. Microbiol.* **9**, 2208 (2018).
- Chan, K. C. et al. Molecular characterization of circulating EBV DNA in the plasma of nasopharyngeal carcinoma and lymphoma patients. *Cancer Res.* **63**, 2028–2032 (2003).
- Greninger, A. L. et al. Clinical metagenomic identification of *Balamuthia mandrillaris* encephalitis and assembly of the draft genome: the continuing case for reference genome sequencing. *Genome Med.* **7**, 113 (2015).
- Mongkolrattanothai, K. et al. Neurobrucellosis: unexpected answer from metagenomic next-generation sequencing. *J. Pediatr. Infect. Dis.* **6**, 393–398 (2017).
- Sardi, S. I. et al. Coinfections of Zika and Chikungunya viruses in Bahia, Brazil, identified by metagenomic next-generation sequencing. *J. Clin. Microbiol.* **54**, 2348–2353 (2016).
- Wilson, M. R. et al. Diagnosing *Balamuthia mandrillaris* encephalitis with metagenomic deep sequencing. *Ann. Neurol.* **78**, 722–730 (2015).

**Publisher's note** Springer Nature remains neutral with regard to jurisdictional claims in published maps and institutional affiliations.

© The Author(s), under exclusive licence to Springer Nature America, Inc. 2020

## Methods

**Ethics.** Study protocols were reviewed and approved by the University of California San Francisco (UCSF) Institutional Review Board (IRB). The majority of residual samples (178 out of 182) were collected in the clinical laboratory with a waiver of consent (UCSF IRB no. 10-01116). A subset of samples ( $n=4$ ) was obtained from patients after consenting them for enrollment in a metagenomic sequencing study (UCSF IRB nos. 15-18425, 17-22051). All experimental methods followed guidelines established by the Helsinki Declaration<sup>57</sup>.

**Sample selection and processing.** All body fluid samples were obtained from patients at UCSF hospitals and clinics between 2017 and 2019. The study used only residual body fluid samples after standard-of-care clinical laboratory testing was performed. Body fluid samples were collected in sterile tubes or using swabs as part of routine clinical care and included abscess, joint, peritoneal, pleural, cerebrospinal, urine, BAL and other fluids (Supplementary Table 1). Swabs were stored in charcoal gel columns (Swab Transport Media Charcoal, no. 220122, BD) and reconstituted in 0.5 ml of Universal Transport Media (350 C, Copan Diagnostics); the medium liquid was subsequently used for culture, PCR and mNGS analyses. Cultures for bacteria, fungi and AFB from body fluid samples were done in-house at UCSF Clinical 16S rDNA and 28S-ITS PCR for bacterial and fungal detection were performed by a reference laboratory at the University of Washington. Residual samples were stored at 4 °C and tested within 14 d of collection, or centrifuged at 16,000 relative centrifugal force (rcf) for 10 min and the supernatant stored at –80 °C until time of extraction.

Plasma samples were obtained by collecting blood from hospitalized patients, as part of routine clinical testing, into EDTA Plasma Preparation Tubes (BD) or standard EDTA Tubes (BD). The tubes were centrifuged (4,000–6,000 rcf for 10 min) within 6 h, and plasma was isolated from the buffy coat and red cells. The plasma component was further aliquoted and centrifuged at 16,000 rcf for 10 min in microcentrifuge tubes. Plasma samples were stored at –80 °C until the time of extraction.

In the study of test performance, body fluids samples were included if culture positive or PCR positive for bacterial or fungal pathogen(s), with pathogen(s) identified to the genus/species level. Body fluids from patients with ambiguous laboratory findings (for example, a positive culture that was judged clinically to be a contaminant) or from patients with an established infectious diagnosis and already receiving targeted treatment at the time of body fluid collection were excluded. Negative control body fluid samples were selected from patients who had clear alternative noninfectious diagnoses (for example, cancer, trauma) and were negative for infection by culture and clinical adjudication (C.Y.C. and W.G.). Parasites were not examined in this study due to the lack of available positive samples at our hospitals located in San Francisco, and the general absence of molecular or serologic testing available to confirm their presence.

In the series of 12 cases, body fluid samples were included if (1) they were culture and PCR negative and (2) from a patient with a microbiologically established infection (by orthogonal testing, such as serology or testing of a different body fluid/tissue) or clinically probable infection based on review of the clinical charts by an infectious disease specialist (C.Y.C.) and clinical pathologist (W.G.) (Table 2).

**DNA extraction.** Samples were processed in a blinded fashion in a Clinical Laboratory Improvement Amendments-certified clinical microbiology laboratory with physically separate pre- and post-PCR rooms. Cells were first removed through centrifugation to minimize host background. Next, 400 µl of body fluid supernatant or plasma underwent total nucleic acid extraction to 60 µl of extract using the EZ1 Advanced XL BioRobot and EZ1 Virus Mini Kit v.2.0 (Qiagen) according to the manufacturer's instructions.

**Library preparation and PCR amplification.** Library preparation was performed using the NEBNext Ultra II DNA Library Prep Kit (New England Biolabs), with the use of 25 µl of extracted DNA input and half of the reagent volumes suggested by the manufacturer's protocol. Briefly, extracted DNA from most samples was quantified on a NanoDrop spectrophotometer (Thermo Fisher) and diluted to 10–100 ng of input as recommended by the manufacturer. Plasma or CSF DNA was not quantified or diluted because typical input concentrations of <10 ng µl<sup>-1</sup> could not be reliably detected using a spectrophotometer. The DNA was then end repaired, ligated with the NEBNext Adapter (0.6 µM final concentration) to enrich for short-fragment pathogen DNA (100–800 nt) relative to residual human genomic DNA (>1 kb) and cleaned using AMPure beads. In addition to the initial manual preparation of 17 samples, an automated protocol using the epMotion 5075 liquid handler (Eppendorf) was used to process the remaining 165 samples, with 16–48 samples batch processed per run.

PCR amplification was performed using a 40-µl mix consisting of adapter-ligated DNA, premixed custom index primers at 3 µM final concentration (Supplementary Table 11) and a quantitative PCR master mix (KAPA RT-kit, no. KK2702, Roche). DNA amplification was performed to saturation of the fluorescent signal on a quantitative PCR (qPCR) thermocycler (Lightcycler 480, Roche) using the following PCR conditions: initiation at 98 °C × 45 s, then 24 cycles of 98 °C × 15 s/63 °C × 30 s/72 °C × 90 s and a final extension step of 72 °C × 60 s.

Cycle threshold (Ct) values were continually monitored until the libraries were fully amplified to saturation. Final DNA libraries were cleaned up using Ampure beads (Beckman) at 0.9× volumetric ratio and eluted in 30 µl of EB buffer (Qiagen).

### Dual-use protocol for Illumina and nanopore sequencing platforms.

Multiplexing barcodes on the Illumina platform typically have a length of 8 nt flanking the sequence read on both ends, but they are not ideal for multiplexing of samples being sequenced on a nanopore instrument (Oxford Nanopore Technologies) due to the higher error rate of this platform. We designed a dual-use barcode system that contained a distinct 37-nt barcode on each side of the sequencing adapter (the first 8 nt of which were used for Illumina multiplexing), which enables sequencing of the multiplexed DNA library on both Illumina and nanopore platforms. The barcodes were designed using an in-house-developed R script to generate 8- and 29-nt barcodes that maximized the Levenshtein distance between any given pair of barcodes. Specifically, the DNA Barcodes package in BioConductor was first used to generate a set of 1,014 unique 10-mers with minimum Levenshtein distance of 4 and a set of 283 unique 8-mers with minimum Levenshtein distance of 3, because computational limitations prevented the direct design of 37-mers. One 8-mer and three 10-mers were then concatenated together with stripping of the last nucleotide to generate a 37-mer index primer; the final set of these 37-mer index primers (total 192) has a mean Levenshtein distance of  $23 \pm 2.4$  s.d. (range 14–31) between any two barcodes (Supplementary Information).

**Illumina sequencing.** DNA libraries were pooled in equal volumes and the sequencing library pool was quantified using the Qubit fluorometer (Thermo Fisher). Illumina sequencing was performed on either a MiSeq (2 × 150-nt paired end, with capacity for up to five samples per run) or HiSeq 1500/2500 instrument (140-nt single or 2 × 140-nt paired end, with capacity for up to 40 samples per lane), according to the manufacturer's protocol.

**Nanopore sequencing.** We adopted stringent procedures to prevent cross-contamination between samples during the library preparation steps, including unidirectional workflow, separation of pre- and post-PCR workspaces and regular cleaning of the workbenches and biosafety cabinets with 5% sodium hypochlorite. Amplified DNA libraries were prepared for nanopore sequencing using the 1D library preparation kit (Oxford Nanopore Technologies) either manually or on an epMotion 5075 liquid handler biorobot (Eppendorf), with processing of 8–16 samples per batch. The input DNA ranged from 200 to 1,000 ng. DNA was then sequenced using either R9.4 or R9.5 flow cells on a MinION or GridION X5 instrument (Oxford Nanopore Technologies). The MinION has a single-flow cell position for processing of a single sample at a time, while the GridION has five flow cell positions for processing of up to five samples simultaneously. Up to five individually barcoded samples per flow cell were sequentially loaded on the nanopore instrument for sequencing. Between each sample, flow cells were washed according to the manufacturer's instructions to minimize carryover contamination. The estimated cost for reagents per sample (excluding labor) was US\$27.20–61.40, and US\$269.70 for Illumina and nanopore sequencing, respectively (Supplementary Information).

**Positive and negative external controls.** Negative controls were derived from the same batch of pooled plasma from healthy donors (Golden West Biologicals). Positive controls consist of the negative control plasma spiked with sheared (to 150–200 base pair range) DNA extracted from cultured nonpathogenic microorganisms (American Type Culture Collection, ATCC): Koi herpesvirus (virus, VT-1592D), *S. uberis* (Gram-positive bacterium, ATCC strain 0140 J BAA-854D-5), *R. sphaeroides* (Gram-negative bacterium, ATCC BAA-808D-5), *M. farinosa* (yeast, ATCC MYA-4447D-5), *A. oryzae* (mold, ATCC 42149D-2) and *Neospora caninum* (parasite, ATCC 50843D) (Supplementary Table 2). All controls underwent the same wet lab procedure and bioinformatics analysis as the clinical samples.

**Limits of detection and linearity.** To evaluate the limit of detection for bacteria and fungi for this assay, we spiked DNA from nonpathogenic microorganisms acquired from ATCC into healthy donor negative plasma in a series of fourfold dilutions from 1:1 (no dilution) to 1:4,096 (Supplementary Table 5). Each concentration of microorganism was tested on mNGS with four replicates for reproducibility. The bacteria and fungi tested include *S. uberis*, *R. sphaeroides*, *M. farinosa* and *A. oryzae*. Thresholds were chosen based on the nRPM corresponding to Youden's index on the training data ROC curve and using the composite standard. The bacterial nRPM thresholds were 2.6 and 0.54 for Illumina and nanopore sequencing, respectively; the fungal nRPM was 0.10 for both Illumina and nanopore sequencing. The LoD was defined as the dilution at which mNGS testing detected the pathogen at levels above the nRPM threshold in four of four replicates.

To evaluate assay linearity, a linear regression was performed on the same four sets of serially diluted positive controls as used in LoD. The nRPM values were plotted against the input concentration (copies or genome equivalents per ml). The best fit regression line, along with the linear equation and  $R^2$  value, were added to the plotted values (Extended Data Fig. 3).

**Bioinformatics analysis.** Illumina sequencing data were analyzed for pathogens using the clinically validated SURPI+ computational pipeline v.1.0.63-dev<sup>7,20,58</sup>. SURPI+ uses the entirety of the NCBI GenBank nucleotide database (March 2015 distribution) as the reference database and incorporates taxonomic classification algorithms for accurate identification of pathogens as previously described<sup>20</sup>. Nanopore sequencing data were analyzed using SURPIrt software (SURPIrt research 1.0.14-build.86)<sup>35</sup>. Raw fast5 files were basecalled using MinKNOW software v.3.1.20 installed on the GridION in real-time mode, without polishing. The basecalled reads were run through in-house-developed scripts for sample demultiplexing using the BLASTn (v.2.7.1+) aligner at a significance threshold of  $10 \times 10^{-2}$ . After trimming of adapters and removing low-quality and low-complexity sequences, the first 450 nt of the preprocessed read was partitioned into three 150-nt segments followed by rapid, low-stringency identification of candidate pathogen reads using SNAP (v.1.0.dev100) alignment to microbial reference databases (viral portion of 2019 NCBI nucleotides; bacterial RefSeq; fungal and parasitic pathogens in the fungal RefSeq and parasitic RefSeq databases)<sup>35</sup>, using an edit distance of 50 (ref. 59). Candidate reads were then filtered and taxonomically classified as previously described<sup>20</sup>. Real-time analysis was performed by running the SURPIrt pipeline in continuously looping mode, with ~100–200 k of nanopore reads analyzed per batch.

**Computational algorithm for pathogen identification.** We developed a pathogen identification algorithm applicable for both Illumina and nanopore datasets outputted by SURPI or SURPIrt (see above) to assess and optimize performance accuracy. An initial reference database was manually tabulated based on pathogens detected in body fluids by culture and/or PCR testing. The algorithm calculated a nRPM pathogen count, filtered out taxonomically related microorganisms and defined criteria for pathogen detection, as explained in detail below.

1. Calculating a normalized RPM. We developed a nRPM metric to standardize microorganisms across samples with uneven sequencing depths and input DNA concentrations. For Illumina sequencing, RPM was defined as the number of pathogen reads divided by the number of preprocessed reads (reads remaining after adapter trimming, low-quality filtering and low-complexity filtering); for nanopore sequencing, RPM was defined as the number of pathogen reads divided by the number of basecalled reads. We then calculated a nRPM that adjusted the RPM with respect to background based on the Ct value (to the nearest 0.5 increment) during the PCR amplification step of library preparation. Because the average Ct value across all samples was 7, nRPM was defined as  $nRPM = RPM/2^{(Ct - 7)}$ . ROC and precision-recall curves were plotted using the Python software package and pandas data analysis library. The optimal nRPM threshold was obtained by plotting the ROC curve at varying nRPM values and determining nRPM at Youden's Index. Our incorporation of a nRPM metric is based on previous observation of a log-linear relationship between the qPCR Ct value and the RPM of representative, presumed background contaminant microorganisms such as *Achromobacter xylosoxidans* (Extended Data Fig. 11). Thus, assuming a constant background level of *A. xylosoxidans*, measured RPM would be inversely correlated with the input concentration as previously reported<sup>60</sup>. In the current study, better performance was achieved using the nRPM versus the RPM metric (Extended Data Fig. 7b,e).
2. Filtering out closely related microorganisms. Taxonomic classification using metagenomics data commonly yields a minority fraction of reads that map to related taxa with the same family or genus as the microorganism truly present in the sample<sup>61</sup>. To minimize cross-species misalignments for closely related microorganisms, we penalized (reduced) the nRPM of microorganisms sharing a genus or family designation. A penalty of 10 and 5% was used for genus and family, respectively, based on the empirical maximization of specificity from the ROC curve of the training set. For example, if *Escherichia coli* had an nRPM of 100 and *Shigella sonnei* (from the same Enterobacteriaceae family) had an nRPM of 5, the nRPM of *S. sonnei* would be reduced to zero. In the current study, better performance was achieved in the training dataset using this filter (Extended Data Fig. 7c).
3. Criteria for pathogen detection. We developed two criteria for pathogen detection. The candidate pathogen was required to (1) have a minimum number of pathogen-specific reads identified ( $\geq 3$  for bacteria and  $\geq 1$  for fungi; Extended Data Fig. 7a,d) and (2) meet an optimal nRPM threshold. Optimal nRPM thresholds using composite standards were set to the maximum Youden's index (bacterial nRPM of 2.6 and 0.54 for Illumina and nanopore sequencing, respectively; fungal RPM of 0.10 for both Illumina and nanopore sequencing), as determined from the ROC curve of the training set. The clinical gold standard (culture/16S PCR) used the same thresholds except that the bacterial nRPM threshold for Illumina sequencing was 3.2.

**Statistical methods.** To evaluate accuracy, we applied two criteria: (1) a clinical gold standard based on culture and 16S PCR results obtained through routine clinical care, and (2) a composite standard based on a combination of clinical testing (culture and 16S/28S-ITS PCR), orthogonal testing (for example, digital PCR, serology) and clinical adjudication. The specific scoring algorithm is outlined

as follows (Supplementary Table 12): based on the clinical or composite standard, true positives or false negatives were scored for each microorganism detected or not detected by mNGS, respectively. For each sample, a true negative was scored if no other microorganism(s) other than those expected, based on the clinical or composite standard, were detected by mNGS; otherwise, a false positive was scored. Multiple false-positive results in a sample were counted as one false positive overall.

We calculated *P* values using a two-sided Welch's *t*-test at a significance threshold of *P*=0.05. All data points in the study were done singly, except for the LoD studies which were performed in four replicates at each dilution.

**Confidence intervals for ROC curves.** To evaluate the reliability of the validation set data, we wrote a custom Python script that bootstrapped our dataset by randomly resampling it with replacement to generate a replicate dataset of the same size for 2,000 iterations. The resultant distribution was used to produce a 95% CI for the ROC curve (Extended Data Fig. 2).

**Orthogonal confirmation of mNGS results.** Digital PCR for orthogonal confirmation of mNGS results was performed using the Biorad QX200 Droplet Digital PCR System. The advantages of dPCR include absolute quantification, improved detection of very-low-abundance nucleic acids with high precision and higher tolerance to the presence of inhibitors and/or contaminants in body fluid samples<sup>62,63</sup>. Thus, the use of dPCR was deemed to be a more robust indicator than conventional PCR for the presence of pathogen-specific DNA in body fluids. All primer and probe pairs were synthesized by Integrated DNA Technologies, and first validated using positive-control microorganisms (Supplementary Table 13). Genomic DNA from positive-control microorganisms was purchased from ATCC and mechanically sheared (MiniTUBE, Covaris) to an average of 200–300 base pairs. For Sanger sequencing, DNA was first cloned into colonies using a TOPO TA Cloning Kit (Thermo Fisher). Sanger sequencing of clones was then performed at Elim Biopharmaceuticals. Sequencing traces were analyzed on Geneious software (v.10.2.3) and aligned to the National Center for Technology Information nucleotide database using BLAST<sup>64</sup>. Serology confirmation in the case of *Bartonella* was performed by Quest Diagnostics.

**Analysis of pathogen and human DNA length.** Pathogen-specific length distributions in mNGS data were obtained by aligning paired-end Illumina reads or single-end nanopore reads to individual pathogen genomes (Extended Data Fig. 6)<sup>36</sup>. For Illumina sequencing data, unaligned, human-depleted FASTQ reads were extracted using the bamtofastq function in the bedtools software package followed by alignment to species-specific microbial reference genomes using the Burrows-Wheeler aligner (BWA). An in-house-developed Python program and Linux shell scripts were used to extract read lengths from resultant paired-end SAM files. For nanopore sequencing data, read lengths were directly extracted from SAM-formatted pathogen reads outputted from the SURPIrt pipeline. Histograms of read length were plotted using the software package Matplotlib as implemented in Python.

For characterization of human DNA length distribution from Illumina data, FASTQ files were first trimmed for Illumina adapters with cutadapt (v.1.16) followed by alignment with BWA (v.0.7.12) to the hg38 human reference genome. This revealed a previously described peak of ~160 nt that corresponds to nuclear DNA wrapped around a single histone (Extended Data Fig. 6a).

Length distributions were assessed from 58 bacterial and ten fungal pathogens by histogram analysis, with the inclusion criteria of at least ten paired-end reads aligned to each pathogen genome (Extended Data Fig. 6b). The average distribution skewed towards shorter length fragments, with a long tail extending to ~700 nt and no significant size differences between bacterial and fungal DNA being observed. This range of pathogen DNA sizes was similar to that previously observed in plasma and urine<sup>65</sup>. Bacterial length distributions from nanopore sequencing were longer on average (356 nt) than from Illumina sequencing (177 nt) (Extended Data Fig. 6c).

**Reporting Summary.** Further information on research design is available in the Nature Research Reporting Summary linked to this article.

## Data availability

Metagenomic sequencing data (FASTQ files) after removal of human genomic reads have been deposited in the NCBI Sequence Read Archive (SRA) (PRJNA558701, under umbrella project PRJNA234047).

## Code availability

SURPI+ v.1.0 (<https://github.com/chulab/SURPI-plus-dist>) and SURPIrt v.1.0 software (<https://github.com/chulab/SURPIrt-dist>) have been deposited on GitHub and are available for download for research use only. Linux (Ubuntu 16.04.6) and Python (python 2.7.12) scripts used for construction of dual-use Illumina and nanopore barcodes are provided in the Supplementary Information, 'Pipeline for Designing 37mer Barcodes'. Other custom scripts for ROC curve and read length analysis have been deposited on Github (<https://github.com/wei2gu/20-NGSInfectedBodyFluids/>).

## References

57. World Medical Association World Medical Association Declaration of Helsinki: ethical principles for medical research involving human subjects. *JAMA* **310**, 2191–2194 (2013).
58. Naccache, S. N. et al. A cloud-compatible bioinformatics pipeline for ultrarapid pathogen identification from next-generation sequencing of clinical samples. *Genome Res.* **24**, 1180–1192 (2014).
59. Zaharia, M. et al. Faster and more accurate sequence alignment with SNAP. Preprint at <https://arxiv.org/abs/1111.5572> (2011).
60. Zinter, M. S., Mayday, M. Y., Ryckman, K. K., Jelliffe-Pawlowski, L. L. & DeRisi, J. L. Towards precision quantification of contamination in metagenomic sequencing experiments. *Microbiome* **7**, 62 (2019).
61. McIntyre, A. B. R. et al. Comprehensive benchmarking and ensemble approaches for metagenomic classifiers. *Genome Biol.* **18**, 182 (2017).
62. Strain, M. C. et al. Highly precise measurement of HIV DNA by droplet digital PCR. *PLoS ONE* **8**, e55943 (2013).
63. Taylor, S. C., Laperriere, G. & Germain, H. Droplet digital PCR versus qPCR for gene expression analysis with low abundant targets: from variable nonsense to publication quality data. *Sci. Rep.* **7**, 2409 (2017).
64. Altschul, S. F., Gish, W., Miller, W., Myers, E. W. & Lipman, D. J. Basic local alignment search tool. *J. Mol. Biol.* **215**, 403–410 (1990).
65. Burnham, P. et al. Urinary cell-free DNA is a versatile analyte for monitoring infections of the urinary tract. *Nat. Commun.* **9**, 2412 (2018).

## Acknowledgements

We thank H. Reyes, A. Chan, D. Ingebrigtsen, L. Dang, W. Lorizio, J. Streithorst, B. Fung and the UCSF clinical laboratory staff for assistance with orthogonal testing. We thank R. Da for assistance with sequencing runs. We thank S. Shiboski for biostatistics feedback. We thank members of the Chiu, Miller and DeRisi laboratories for feedback and support. This work was funded in part by an NIH grant (no. K08-CA230156) and a Burroughs-Wellcome Award to W.G., by Abbott Laboratories (C.Y.C.), a NIH/NHLBI grant (no. R01-HL105704, to C.Y.C.), a NIH/NIAID grant (no. R33-AI120977, to C.Y.C.), the California Initiative to Advance Precision Medicine (C.Y.C.), a UC Center for Accelerated Innovation grant funded by NIH grant U54HL119893 and NIH/

NCATS UCSF-CTSI grant UL1TR000004 (C.Y.C.), and the Charles and Helen Schwab Foundation (C.Y.C.).

## Author contributions

W.G., X.D. and C.Y.C. conceived and designed the study. W.G., X.D. and C.Y.C. coordinated the study. W.G., X.D., M.L., Y.D.S., S.A., A.G., K.R., G.Y., B.B., E.D.C., C.W. and E.H. performed experiments. W.G., X.D., M.L., E.H. and C.Y.C. analyzed data. W.G., G.I., E.H. and C.Y.C. reviewed patient electronic medical records. S.E. and D.S. wrote software and performed SURPI bioinformatics analysis of mNGS data. K.Z., H.S. and G.I. enrolled patients in the study and assisted in patient data collection. A.B., M.R.W., S.M., J.L.D. and C.Y.C. provided clinical samples and resources. W.G., X.D., M.L. and C.Y.C. wrote and edited the manuscript. W.G. and C.Y.C. designed the figures. C.Y.C. supervised the study. All authors read the manuscript and agree to its contents.

## Competing interests

C.Y.C. is the director of the UCSF-Abbott Viral Diagnostics and Discovery Center and receives research support funding from Abbott Laboratories, Inc. C.Y.C., D.S., S.F. and S.M. are inventors on a patent application on algorithms related to SURPI+ software (no. PCT/US/16/52912, 'Pathogen Detection using Next-Generation Sequencing'). C.Y.C., X.D. and S.F. are inventors on a patent pending on algorithms related to SURPIrt software (Case no. SF2015-154, 'Methods for Real-Time Sequencing Analysis of Infectious Diseases'). Other coauthors declare no competing interests.

## Additional information

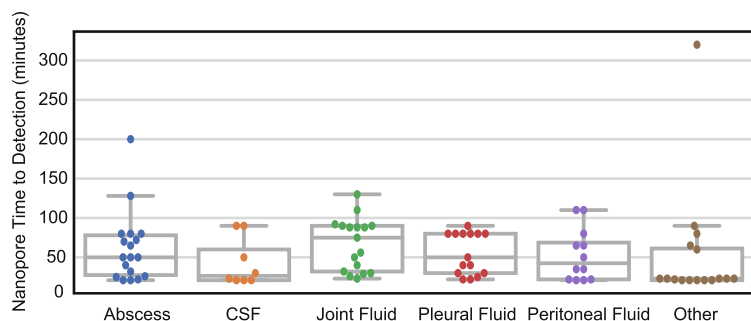
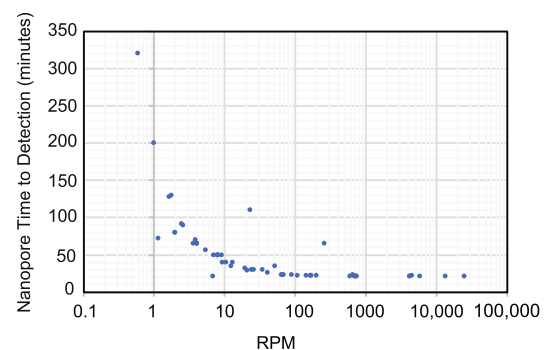
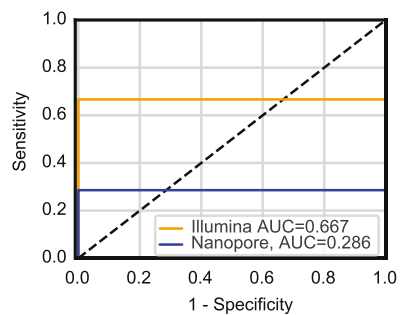
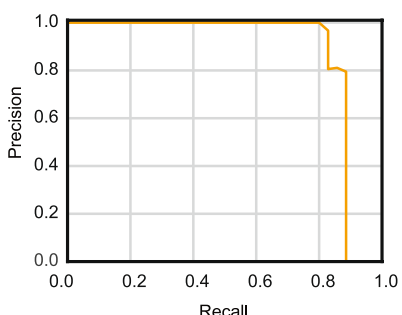
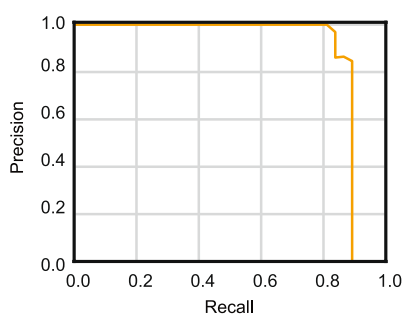
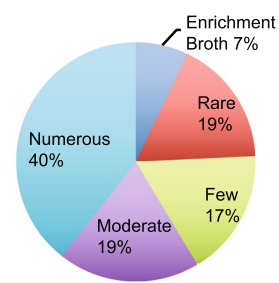
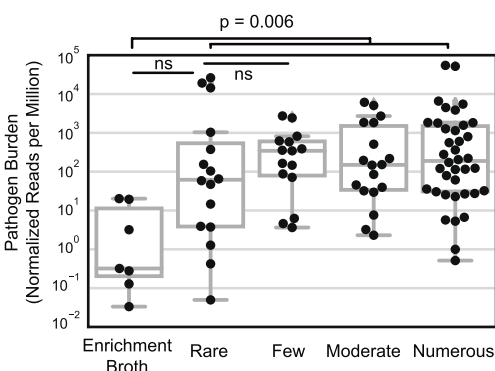
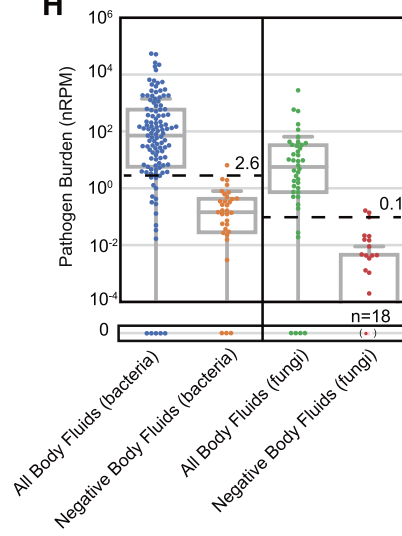
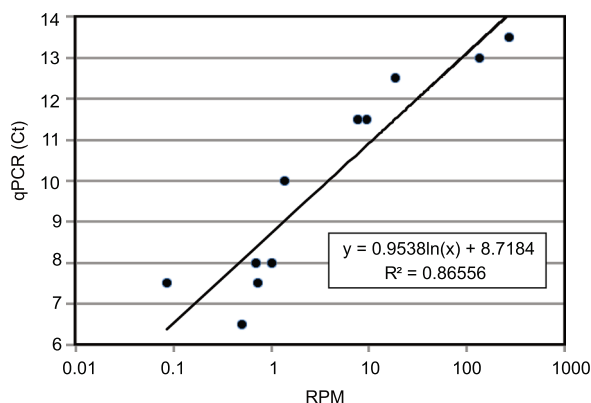
**Extended data** is available for this paper at <https://doi.org/10.1038/s41591-020-1105-z>.

**Supplementary information** is available for this paper at <https://doi.org/10.1038/s41591-020-1105-z>.

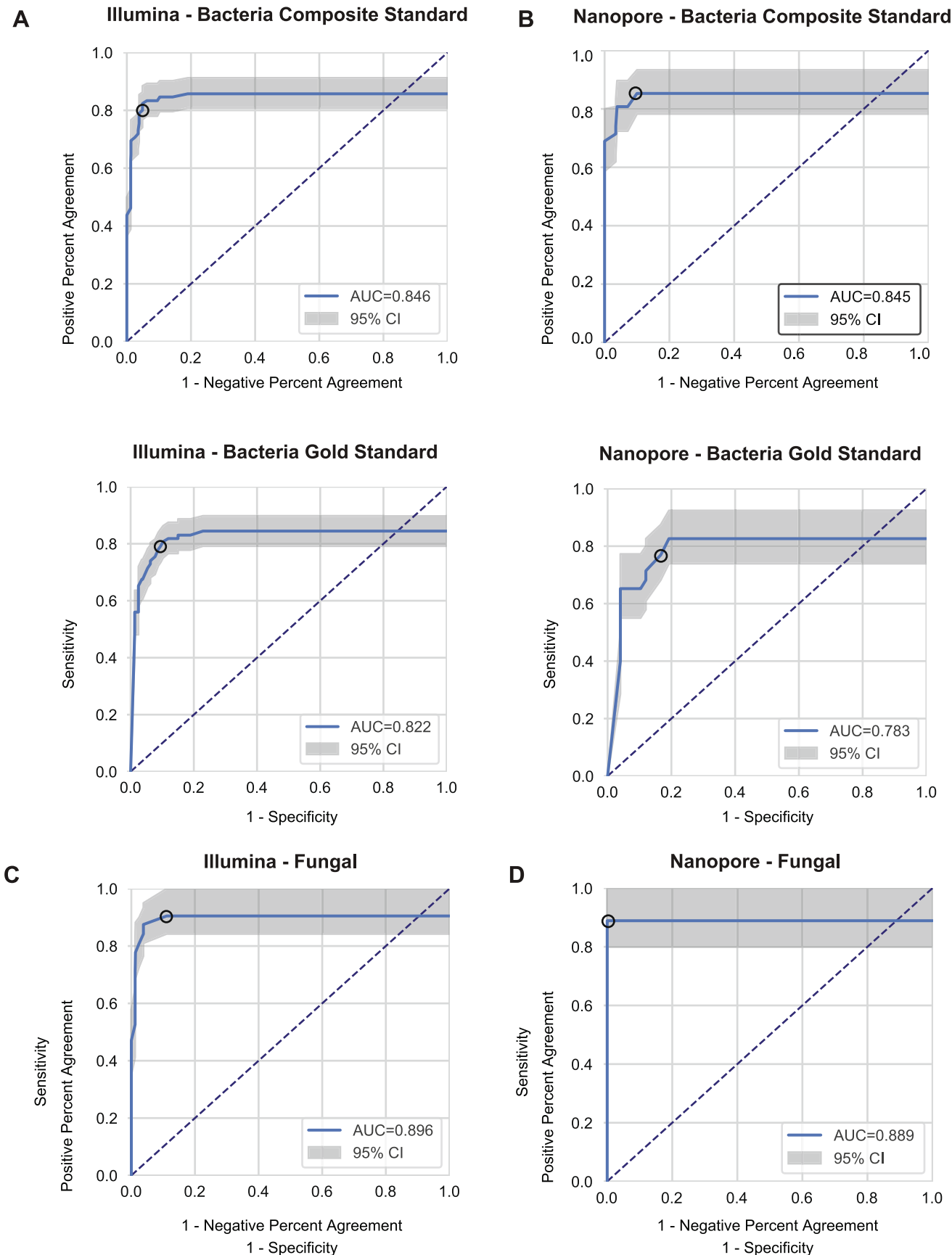
**Correspondence and requests for materials** should be addressed to C.Y.C.

**Peer review information** Alison Farrell is the primary editor on this article and managed its editorial process and peer review in collaboration with the rest of the editorial team.

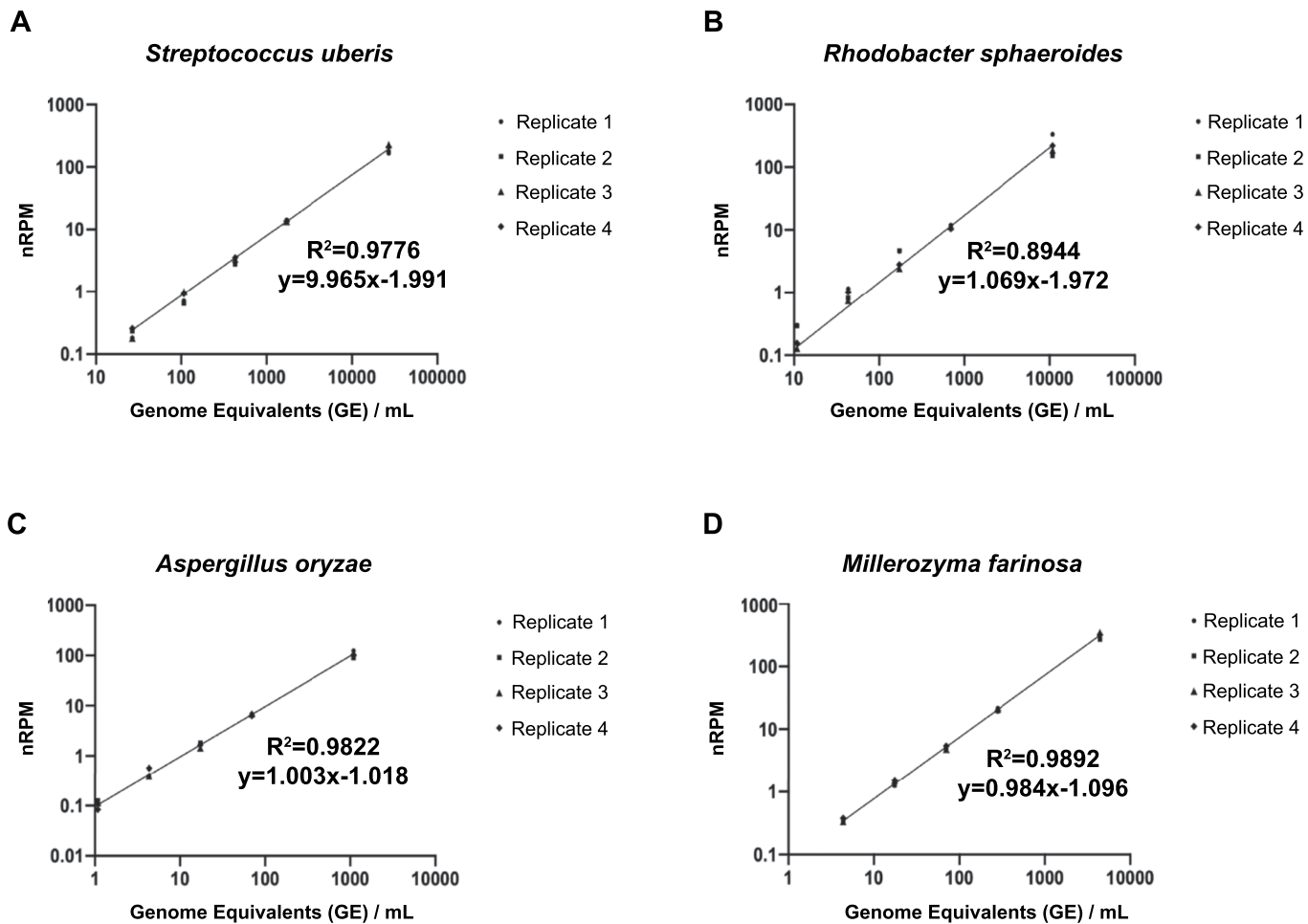
**Reprints and permissions information** is available at [www.nature.com/reprints](http://www.nature.com/reprints).

**A****B****C****D****E****F****G****H****I****Extended Data Fig. 1 | See next page for caption.**

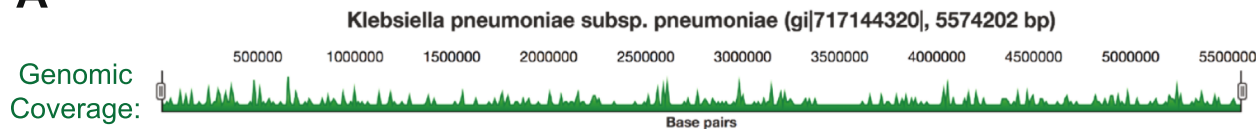
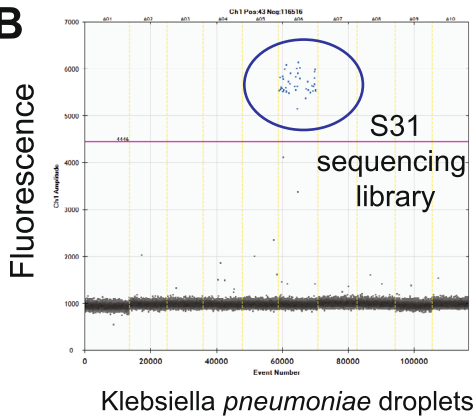
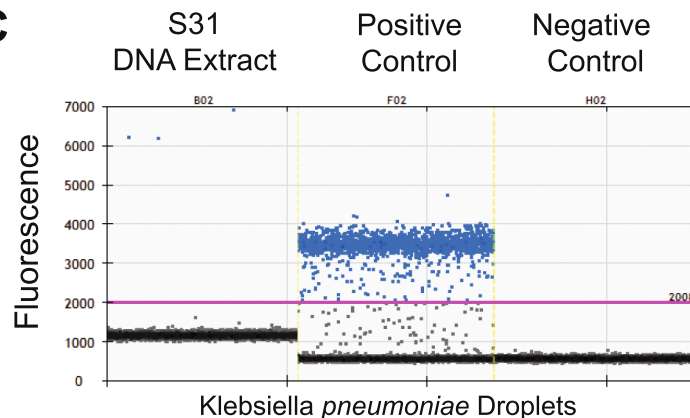
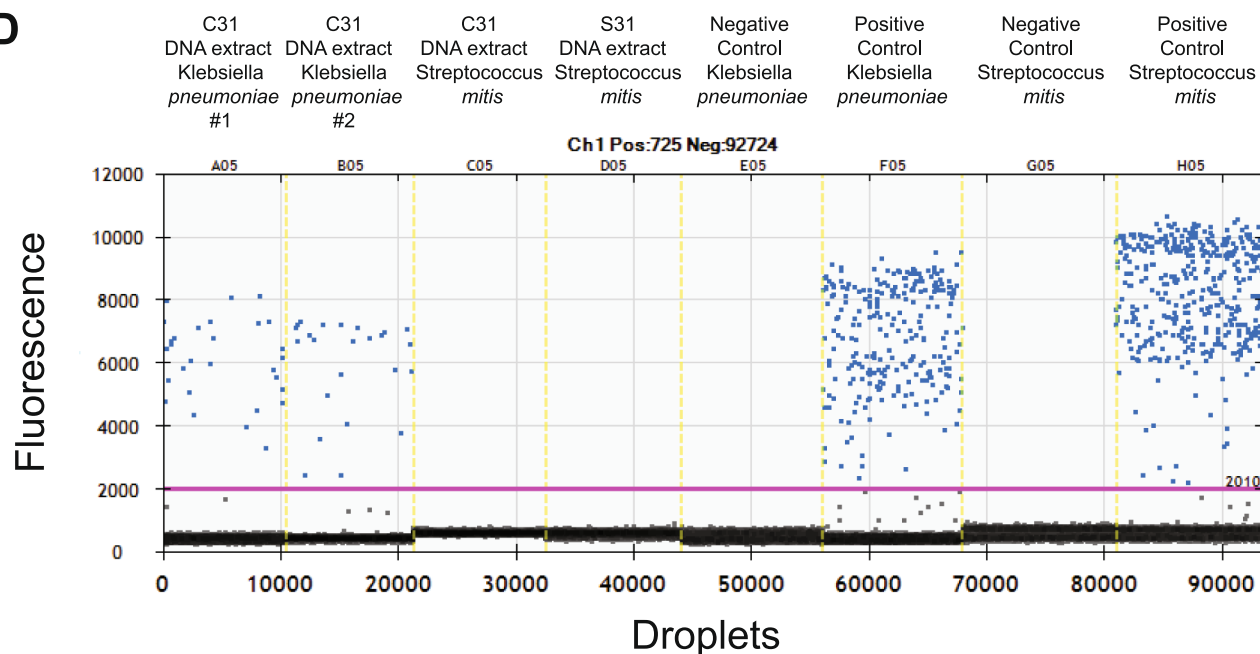
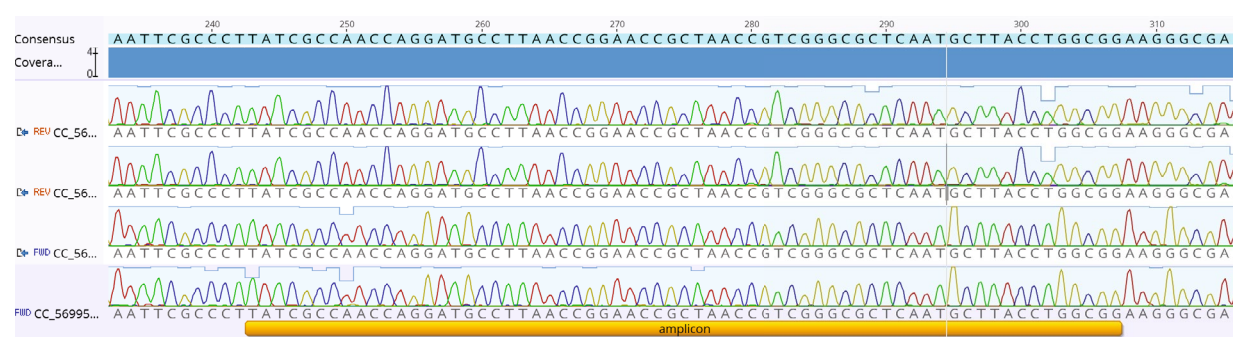
**Extended Data Fig. 1 | Metagenomic sequencing of body fluids.** **a**, Nanopore time to detection (minutes) across different body fluid types. Each data point represents the time to detection of the organism, if any, in each body fluid sample. **b**, Nanopore time to detection (minutes) in relation to pathogen DNA abundance in samples (reads per million, RPM). All box plots represent the median (centre), the interquartiles (minima and maxima), and 1.5 x interquartile range (whiskers). **c**, Precision-recall curves for Illumina and nanopore training fungal datasets. **d**, Precision-recall curves based on the Illumina training bacterial dataset in comparison with the composite standard. **e**, Precision-recall curves based on nanopore bacterial training datasets. **f**, Pie chart showing distribution of bacterial pathogen titers as estimated by semi-quantitative culture. **g**, Plot of nRPM values versus semi-quantitative bacterial titers. The nRPM corresponding to bacteria cultured in enrichment broth was significantly lower than the other higher-titer cultures ( $p=0.006$ ). **h**, Relative pathogen burden in positive and negative (non-infectious) body fluid samples. **i**, Log scale plot of the bacterium *Achromobacter xylosoxidans* from mNGS data, a common background contaminant in sequencing libraries. There is a log-linear relationship between the qPCR cycle threshold (Ct) value and the RPM corresponding to *Achromobacter xylosoxidans*. The background level of *Achromobacter xylosoxidans* is inversely correlated with the input concentration and is relatively constant.



**Extended Data Fig. 2 | ROC curves of mNGS test performance.** ROC curves are plotted from validation set data based on a clinical gold standard or composite standard. Data are presented as median true positive rates  $\pm$  the 95% confidence intervals. The 95% confidence interval was obtained via a bootstrap method with 2000 resampling iterations. **a**, Illumina dataset, bacterial detection ( $n=127$  samples). **b**, Nanopore dataset, bacterial detection ( $n=43$  samples). **c**, Illumina dataset, fungal detection ( $n=127$ , 32 fungal organisms). **d**, Nanopore dataset, fungal detection ( $n=43$ , 11 fungal organisms).

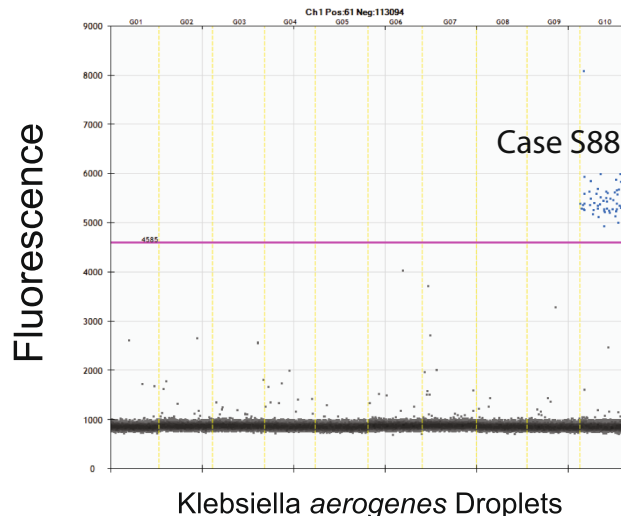
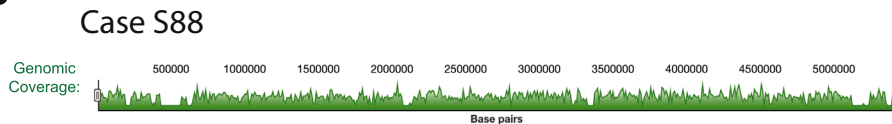
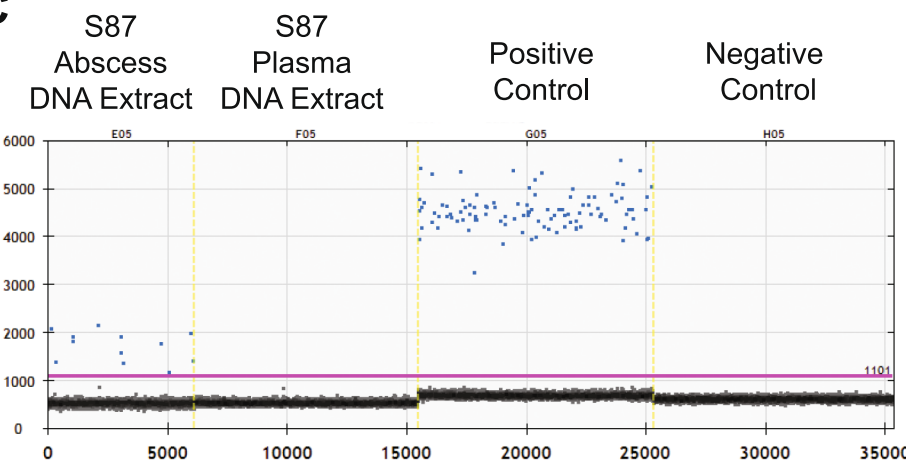


**Extended Data Fig. 3 | Relationship of external positive control organism titer with mNGS detection signal (expressed in nRPM).** Simple linear regression of normalized reads per million (nRPM) over four replicates per dilution factor, calculated as genome equivalents per mL (GE/mL) for **a**, *Streptococcus uberis*, **b**, *Rhodobacter sphaeroides*, **c**, *Aspergillus oryzae*, and **d**, *Millerozyma farinosa*.

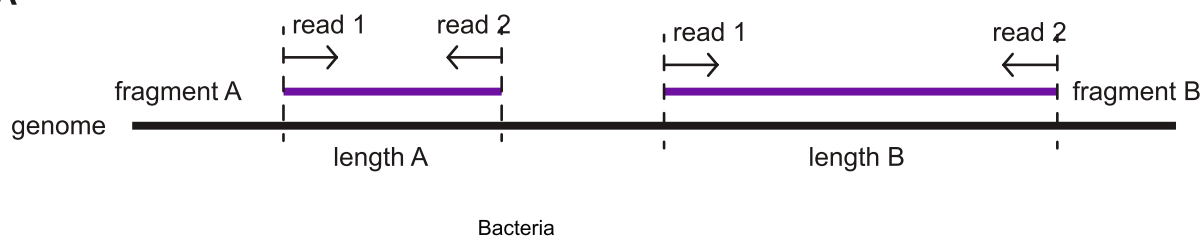
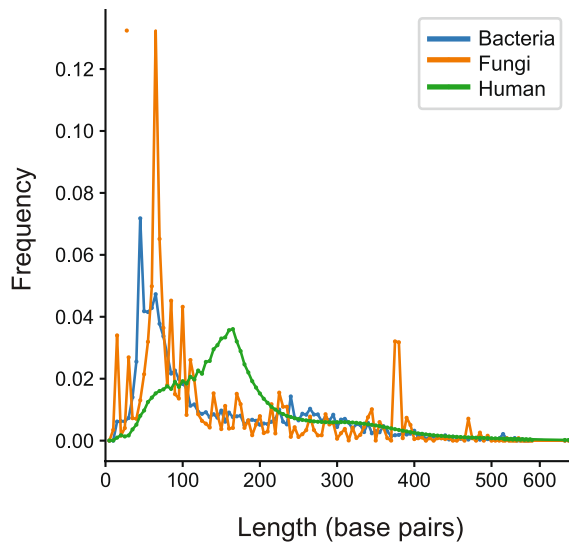
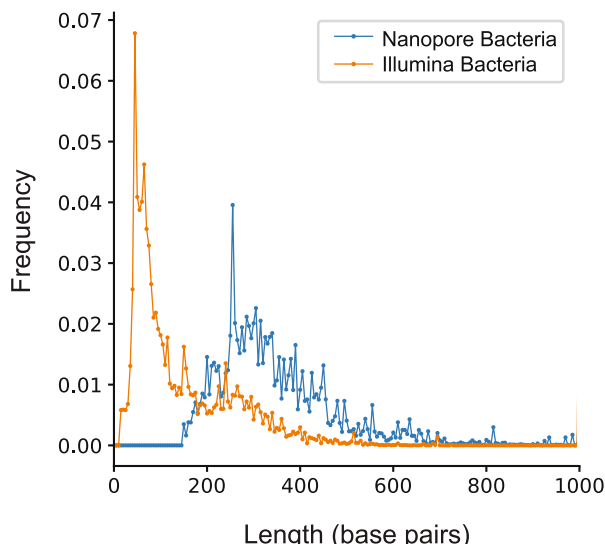
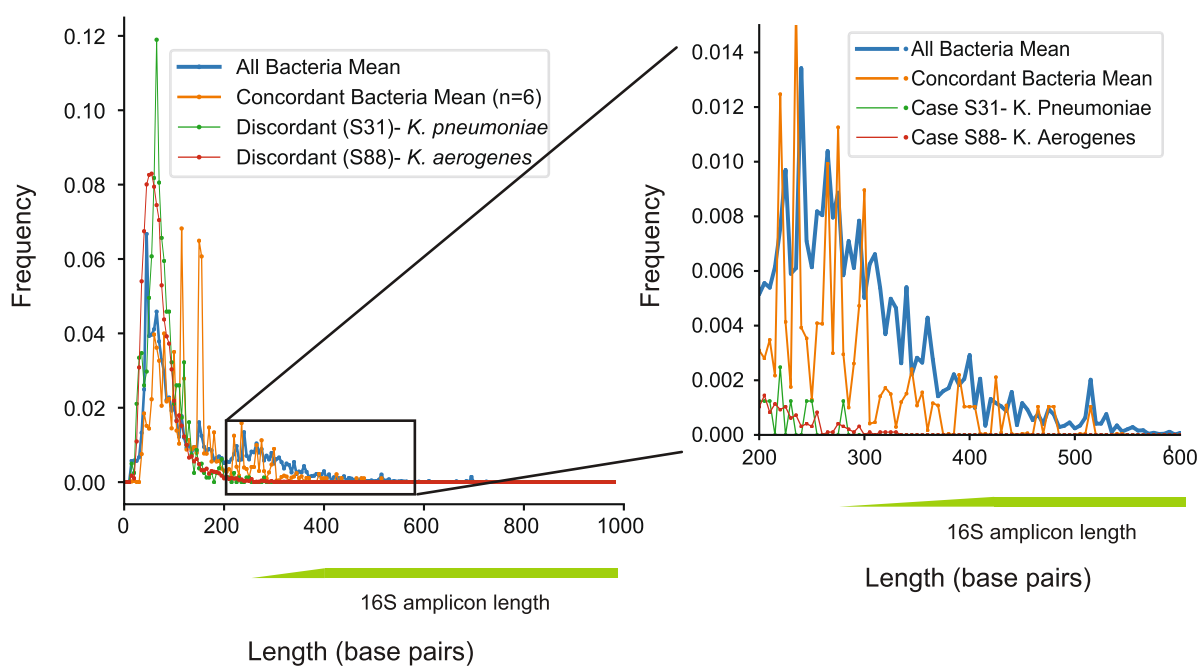
**A****B****C****D****E**

Extended Data Fig. 4 | See next page for caption.

**Extended Data Fig. 4 | Orthogonal testing for Case S31: *Klebsiella pneumoniae* infection of pleural fluid.** **a**, Genomic coverage of *K. pneumoniae* from Illumina mNGS. Sequencing spanned 36,490 base pairs, or 0.65% of the *K. pneumoniae* genome. **b**, Orthogonal confirmation of *K. pneumoniae* by dPCR of the sequencing library. Nine negative controls from other cases were run in parallel. Out of 10 sequencing libraries, only Case S31 had any positive droplets ( $n=43$  of 12022 total droplets as circled). **c**, Orthogonal confirmation of *K. pneumoniae* by dPCR of the DNA extract. Three positive droplets were detected, indicating a low positive result. **d**, Orthogonal confirmation of *K. pneumoniae* by dPCR of contralateral pleural fluid (sample C31). 29 and 24 positive droplets were detected out of 2 replicates. Digital PCR targeting *Streptococcus mitis* on both pleural fluids did not yield any positive droplets. The positive controls for these experiments were from sheared DNA from *Klebsiella pneumoniae* and *Streptococcus mitis* respectively, whereas the negative control was water. **e**, Sanger sequencing of the *K. pneumoniae* amplicon from dPCR. Shown are sequencing traces confirming the presence of *K. pneumoniae*.

**A****B****C**
**Extended Data Fig. 5 | Orthogonal testing for Cases S88: *Klebsiella aerogenes* from cerebrospinal fluid and S87: *Bartonella henselae* from a skin abscess.**

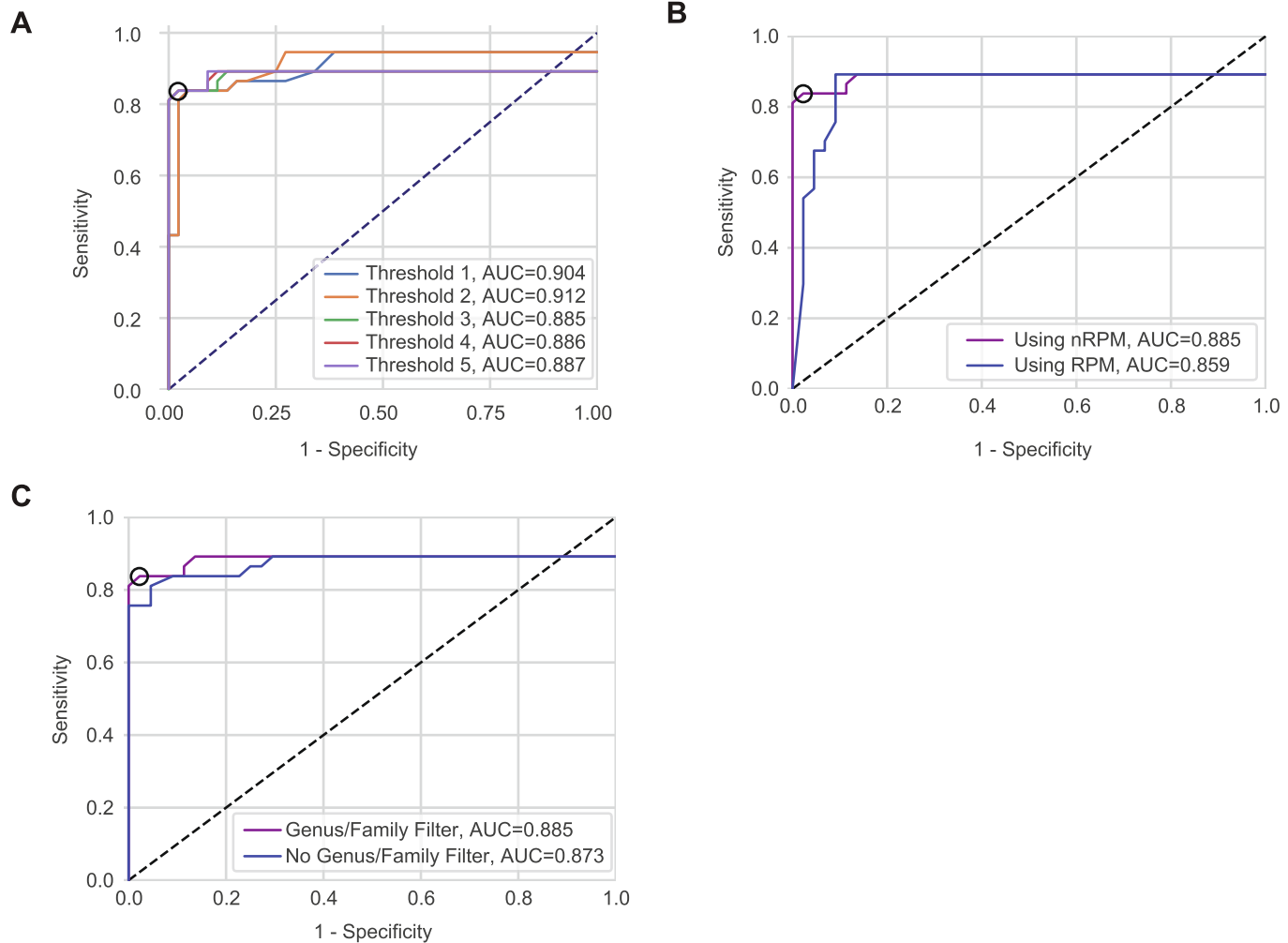
**a**, Orthogonal confirmation of *K. aerogenes* by dPCR of the DNA extract. The sample was run in parallel with 9 negative controls. Out of 10 sequencing libraries, only Case S88 had positive dPCR droplets ( $n=61$ ). **b**, Genomic coverage of *K. aerogenes* from Illumina mNGS. The assembled genomic regions spanned 536,461 bp, or 9.9% of the bacterial genome. **c**, Orthogonal confirmation of *Bartonella henselae* by dPCR of the DNA extract. Positive dPCR droplets ( $n=12$ ) are seen in abscess fluid and the positive control consisting of sheared DNA from *Bartonella henselae* (ATCC 49882). The negative control was water.

**A****B****C****D**

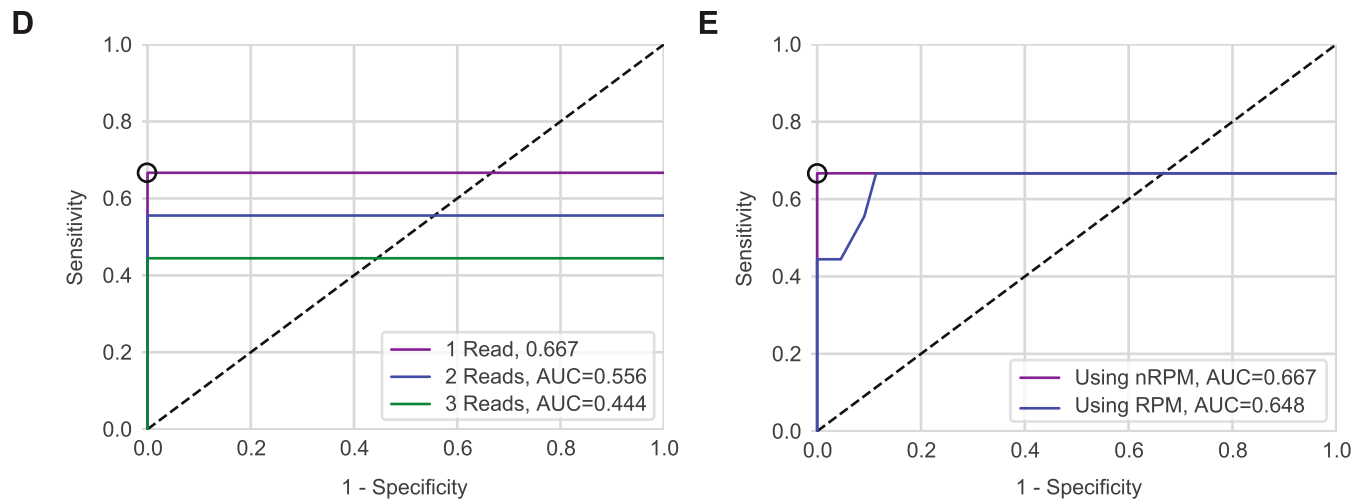
Extended Data Fig. 6 | See next page for caption.

**Extended Data Fig. 6 | Length distributions of pathogen cfDNA in mNGS data.** Analysis is performed on the 87 body fluid samples sequenced on both Illumina and nanopore platforms. **a**, Diagram showing how original genomic DNA lengths are recovered. Paired-end sequencing data is aligned to either a human or microbial genome, followed by determination of fragment length from the start and end positions and construction of a read length histogram. **b**, Histogram of average DNA lengths for human, bacterial, and fungal organisms obtained from mNGS data. Human DNA is observed to peak at the stereotypical 160 bp nucleosome footprint; both bacterial and fungal DNA are most abundant at sizes of <100 bp, but a higher molecular weight tail is observed extending to 500–600 bp. **c**, Histogram of bacterial read lengths according to sequencing platform. Illumina and nanopore sequencing platforms produce different size distributions. **d**, Length analysis of mNGS reads for samples with 16S PCR performed. Comparison of the length profiles of the 16S discordant bacteria cases (S31 and S88), 16S concordant bacteria cases (mean of S10, S36, S41, S69, S85, S128), and all bacteria mean. The pathogen cfDNA in cases S31 and S88 are more fragmented, with the vast majority of fragments <300 bp. The relative paucity of longer fragments could hinder 16S PCR amplification.

## BACTERIAL TRAINING



## FUNGAL TRAINING



Extended Data Fig. 7 | See next page for caption.

**Extended Data Fig. 7 | Comparison of different threshold variables on the training set to calibrate the thresholds for each variable used.** The final thresholds used are circled in each ROC chart. **a**, Comparison of different minimal read thresholds for bacteria calling. Based on this data and prior selection of minimal reads, we selected a minimal of 3 reads for the validation set. **b**, Comparison of using or not using a PCR Ct value normalization for bacteria calling. Normalization resulted in higher specificity and was used on the validation set. **c**, Comparison of using a same-genus/same-family filter to decrease an informatics artifact where a pathogen burden is high and related species would appear at significant lower values. Using this filter improved specificity. **d**, Comparison of different minimal read thresholds for fungal calling. We selected a minimal of 1 read based on the significantly higher sensitivity at the lowest threshold. **e**, Comparison of using or not using a PCR Ct value normalization for fungal calling. Normalization resulted in higher specificity and was used on the validation set.

Corresponding author(s): Charles Chiu

Last updated by author(s): Aug 20, 2020

## Reporting Summary

Nature Research wishes to improve the reproducibility of the work that we publish. This form provides structure for consistency and transparency in reporting. For further information on Nature Research policies, see [Authors & Referees](#) and the [Editorial Policy Checklist](#).

### Statistics

For all statistical analyses, confirm that the following items are present in the figure legend, table legend, main text, or Methods section.

n/a Confirmed

- The exact sample size ( $n$ ) for each experimental group/condition, given as a discrete number and unit of measurement
- A statement on whether measurements were taken from distinct samples or whether the same sample was measured repeatedly
- The statistical test(s) used AND whether they are one- or two-sided  
*Only common tests should be described solely by name; describe more complex techniques in the Methods section.*
- A description of all covariates tested
- A description of any assumptions or corrections, such as tests of normality and adjustment for multiple comparisons
- A full description of the statistical parameters including central tendency (e.g. means) or other basic estimates (e.g. regression coefficient) AND variation (e.g. standard deviation) or associated estimates of uncertainty (e.g. confidence intervals)
- For null hypothesis testing, the test statistic (e.g.  $F$ ,  $t$ ,  $r$ ) with confidence intervals, effect sizes, degrees of freedom and  $P$  value noted  
*Give  $P$  values as exact values whenever suitable.*
- For Bayesian analysis, information on the choice of priors and Markov chain Monte Carlo settings
- For hierarchical and complex designs, identification of the appropriate level for tests and full reporting of outcomes
- Estimates of effect sizes (e.g. Cohen's  $d$ , Pearson's  $r$ ), indicating how they were calculated

*Our web collection on [statistics for biologists](#) contains articles on many of the points above.*

### Software and code

Policy information about [availability of computer code](#)

Data collection

No software was used for data collection.

Data analysis

Software accessibility: SURPI+ v1.0 (<https://github.com/chiulab/SURPI-plus-dist>) and SURPIrt v1.0 (<https://github.com/chiulab/SURPIrtdist>) have been deposited on GitHub and are available for download for research use only. Fast5 files were basecalled using MinKNOW software v3.1.20 installed on the GridION, and the BLASTn aligner (v2.7.1+) was used for sample demultiplexing. Code accessibility: Linux (Ubuntu 16.04.6) and Python scripts (python 2.7.12) used for construction of dual-use Illumina and nanopore barcodes are provided in the Supplementary Material, "Pipeline for Designing 37mer Barcodes". Other scripts for analysis and figure data files are located at: <https://github.com/wei2gu/2020-NGSInfectedBodyFluids>.

For manuscripts utilizing custom algorithms or software that are central to the research but not yet described in published literature, software must be made available to editors/reviewers. We strongly encourage code deposition in a community repository (e.g. GitHub). See the Nature Research [guidelines for submitting code & software](#) for further information.

### Data

Policy information about [availability of data](#)

All manuscripts must include a [data availability statement](#). This statement should provide the following information, where applicable:

- Accession codes, unique identifiers, or web links for publicly available datasets
- A list of figures that have associated raw data
- A description of any restrictions on data availability

Metagenomic sequencing data (FASTQ files) after removal of human genomic reads have been deposited into the NCBI Sequence Read Archive (SRA) with accession numbers available under PRJNA558701 (umbrella Bioproject PRJNA234047). NCBI GenBank nt database and RefSeq database were used to build SURPI+ or SURPIrt classification database respectively.

# Field-specific reporting

Please select the one below that is the best fit for your research. If you are not sure, read the appropriate sections before making your selection.

- Life sciences       Behavioural & social sciences       Ecological, evolutionary & environmental sciences

For a reference copy of the document with all sections, see [nature.com/documents/nr-reporting-summary-flat.pdf](https://nature.com/documents/nr-reporting-summary-flat.pdf)

## Life sciences study design

All studies must disclose on these points even when the disclosure is negative.

Sample size	All body fluid samples were collected retrospectively from the clinical laboratory, along with clinical data. Convenience sampling for collection of positive control body fluids was performed based on availability (sufficient residual volume after clinical testing was completed).
Data exclusions	No experimental data were excluded. There were inclusion and exclusion criteria for body fluid samples as described in the manuscript.
Replication	Both Illumina and Nanopore mNGS was performed once per sample. For the limit of detection analysis, 4 replicates were performed for each dilution.
Randomization	Randomization of clinical specimens was performed to determine the training and validation experimental groups for the accuracy study.
Blinding	Sample processing, preparation, sequencing, and metagenomic analysis were performed blinded. Multiple iterations to optimize the performance thresholds of the training set required unblinded knowledge of the gold standard results. Analysis of the validation sets were performed blinded. Determining the composite standard was not a blinded process because discordant results between mNGS and traditional microbiological testing required orthogonal testing (e.g. targeted PCR).

## Reporting for specific materials, systems and methods

We require information from authors about some types of materials, experimental systems and methods used in many studies. Here, indicate whether each material, system or method listed is relevant to your study. If you are not sure if a list item applies to your research, read the appropriate section before selecting a response.

Materials & experimental systems	Methods
n/a	Involved in the study
<input checked="" type="checkbox"/>	<input type="checkbox"/> Antibodies
<input checked="" type="checkbox"/>	<input type="checkbox"/> Eukaryotic cell lines
<input checked="" type="checkbox"/>	<input type="checkbox"/> Palaeontology
<input checked="" type="checkbox"/>	<input type="checkbox"/> Animals and other organisms
<input type="checkbox"/>	<input checked="" type="checkbox"/> Human research participants
<input checked="" type="checkbox"/>	<input type="checkbox"/> Clinical data
n/a	Involved in the study
	<input checked="" type="checkbox"/> ChIP-seq
	<input checked="" type="checkbox"/> Flow cytometry
	<input checked="" type="checkbox"/> MRI-based neuroimaging

## Human research participants

Policy information about [studies involving human research participants](#)

Population characteristics	Please see Table 1 for a summary of patient and sample characteristics. Briefly, among the 158 patients with available clinical data, 144 (91%) were hospitalized, of whom 61 (39%) required intensive care unit (ICU) management and 45 (28%) met clinical criteria for sepsis, 51 (32%) were immunocompromised and 71 (45%) were on antibiotics at the time of body fluid collection.
Recruitment	All body fluid samples were obtained from patients at the University of California San Francisco (UCSF) hospitals and clinics between 2017–2019. The study only used residual body fluid samples after standard-of-care laboratory testing was performed. Selection bias against slow-growing organisms (e.g. mycobacteria, molds) may occur due to the limited storage duration of residual samples, which may be less than the organism's time to positivity by culture. Self-selection bias may also affect results as certain fluid types are less available in volume than others (e.g. ocular/eye fluids versus peritoneal fluid). Therefore, results are less generalizable for body fluids that are available at lower volumes.
Ethics oversight	Study protocols were reviewed and approved by the UCSF Institutional Review Board (IRB). The majority of residual samples (178 out of 182) were collected in the clinical laboratory with a waiver of consent (UCSF IRB #10-01116). A subset of samples (n=4) were obtained from patients after consenting them for prospective enrollment in a metagenomic sequencing study (UCSF IRB #15-18425, 17-22051). All experimental methods followed guidelines established by the Helsinki Declaration.

Note that full information on the approval of the study protocol must also be provided in the manuscript.